NASA Reference Publication

1996

Meteor–3 Total Ozone Mapping Spectrometer (TOMS) Data Products User's Guide

Jay R. Herman, P. K. Bhartia,
Arlin J. Krueger, and Richard D. McPeters
NASA/Goddard Space Flight Center
Greenbelt, MD 20771

Charles G. Wellemeyer, Colin J. Seftor,
Glen Jaross, Barry M. Schlesinger,
Omar Torres, Gordon Labow,
William Byerly, Steven L. Taylor, Tom Swissler,
Richard P. Cebula, and Xiao-Yue Gu
Hughes STX Corporation (HSTX)
4400 Forbes Boulevard
Lanham, MD 20706

National Aeronautics and Space Administration

Scientific and Technical Information Branch

ACKNOWLEDGMENTS

The Level–2 and Level–3 data products described in this User's Guide were prepared by the Ozone Processing Team (OPT) of NASA/Goddard Space Flight Center. Please acknowledge the Ozone Processing Team as the source of these data whenever reporting on results obtained using the TOMS data.

The TOMS algorithm development, evaluation of instrument performance, ground-truth validation, and data production were carried out by the Ozone Processing Team (OPT) at NASA/GSFC. The OPT is managed by the Nimbus Project Scientist, R. D. McPeters. The current OPT members include Z. Ahmad, E. Beach, P. Bhartia, W. Byerly, R. Cebula, E. Celarier, S. Chandra, M. DeLand, D. Flittner, L. Flynn, J. Gleason, X. Gu, J. Herman, E. Hilsenrath, S. Hollandsworth, C. Hsu, R. Hudson, G. Jaross, A. Krueger, G. Labow, D. Larko, J. Miller, L. Moy, R. Nagatani, P. Newman, H. Park, W. Planet, D. Richardson, C. Seftor, T. Swissler, J. Stokes, R. Stolarski, S. Taylor, O. Torres, and C. Wellemeyer.

The TOMS instrument was built by Beckman Instruments, Inc., of Anaheim, California, and adapted for use aboard the Russian Meteor–3 Spacecraft by Perkin Elmer Corp. at Pomona, California.

TABLE OF CONTENTS

TABLE OF CONTENTS (Continued)

LIST OF FIGURES

LIST OF TABLES

LIST OF TABLES (Continued)

1.0 INTRODUCTION

This document is a guide to the data products derived from the measurements made by the Total Ozone Mapping Spectrometer (TOMS) experiment aboard the Meteor–3 satellite, and processed by the National Aeronautics and Space Administration (NASA). It discusses the calibration of the instrument, the algorithm used to derive ozone values from the measurements, uncertainties in the data, and the organization of the data products. The data begin August 22, 1991 and end December 28, 1994. These data are archived at the Goddard Space Flight Center (GSFC) Distributed Active Archive Center (DAAC). Meteor–3 data have been processed independently by the Central Aerological Observatory (CAO) of the Russian State Committee on Hydrometeorology (Hydromet); that processing and its products are not discussed in this document.

Long-term trends in atmospheric ozone can be determined most accurately if there is substantial overlap in time between data sets from successive ozone monitoring instruments. In addition, because of the appearance of the Antarctic ozone hole, there has been significant interest in monitoring the behavior of this hole and in monitoring the Arctic for possible appearance of an analogous spring depletion. The Meteor–3/TOMS program was conceived to accomplish these tasks and to foster scientific cooperation between the Soviet Union and the United States. The integration and launch of the Meteor–3/TOMS mission has represented a major step forward in cooperative space projects between the United States and the former Soviet Union. The one and a half year overlap between Nimbus–7 and Meteor–3 has permitted an intercalibration that allows the data from the two satellites to be used to form a continuous 16-year data set that can be used to derive ozone trends from November 1978 through December 1994.

To carry out this program, the Nimbus–7 TOMS Engineering Model, FM2 was refurbished to flight status. An Interface Adapter Model (IAM) was added to make the TOMS instrument, which had been designed to operate with Nimbus, compatible with Meteor–3. The other significant change was the replacement of the single diffuser with a three diffuser carousel, which allowed calibration by comparison of diffusers with different rates of exposure.

Meteor–3 was launched on August 15, 1991; ozone measurements began about 8 days later. For the purpose of obtaining daily high-resolution global maps of atmospheric ozone, Meteor–3/TOMS measured the solar irradiance and the radiance backscattered by the Earth's atmosphere in six selected wavelength bands in the ultraviolet. It scanned the Earth in 3-degree steps to 51 degrees on each side of the subsatellite point in a direction perpendicular to the orbital plane. Consecutive cross-scans overlapped, creating a contiguous mapping of ozone.

The algorithm used to retrieve total column ozone (also referred to as total ozone) from these radiances and irradiances is outlined in Section 2.2 and described in detail in Section 4. This algorithm is identical to the one used for the Version 7 Nimbus–7 TOMS data archive. Because of this, the initial archive of the Meteor–3 TOMS data set is also referred to as Version 7. A radiative transfer model is used to calculate backscattered radiances as a function of total ozone, latitude, viewing geometry, and reflecting surface conditions. Ozone can then be derived by comparing measured radiances with theoretical radiances calculated for the conditions of the measurement and finding the value of ozone that gives a computed radiance equal to the measured radiance.

Section 2 provides a general overview of the Meteor–3/TOMS instrument, the algorithm, the uncertainties in the results, and of other basic information required for best use of the data files. It is designed for the user who wants a basic understanding of the products but does not wish to go into all the details. Such a user may prefer to read only those parts of Sections 3 through 6 addressing questions of particular interest. In Section 3, the instrument, its calibration, and the characterization of its changes with time are discussed. The algorithm for retrieval of total ozone and its theoretical basis are described in Section 4. Section 5 describes the overall uncertainties in the ozone data and how they are estimated, while Section 6 discusses particular problems that may produce errors in specific time intervals and geographical areas. Both sections identify some anomalies remaining in the data and discuss what is known about them. The structure of the data products is identical to those of Nimbus–7 TOMS. This information is presented in Section 7. Appendix A tabulates the standard atmospheric ozone and temperature profiles used in the algorithm for ozone retrieval. Appendix B describes software available for reading the data files, and Appendix C provides information on data availability.

2.0 OVERVIEW

2.1 Instrument

The TOMS experiment on board the Meteor–3 satellite provided daily global coverage of the Earth's total ozone by measuring the backscattered Earth radiance in the six 1-nm bands listed in Table 3.1. The experiment used a single monochromator and scanning mirror to sample the backscattered solar ultraviolet radiation at 35 sample points at 3-degree intervals along a line perpendicular to the orbital plane. Figure 2.1 illustrates the resulting instantaneous fields of view (IFOV) on the Earth's surface for adjacent scans and adjacent orbits. In normal operation, the scanner measured 35 scenes, one for each scanner view angle stepping from right to left. It then quickly returned to the first position, not making measurements on the retrace. Eight seconds after the start of the previous scan, another would begin. The measurements used for ozone retrieval were made during the sunlit portions of the orbit. The instrument operated continuously.

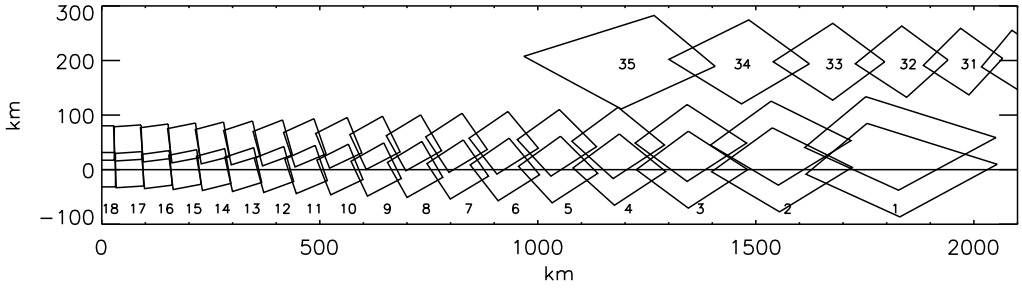

Figure 2.1 Meteor-3 TOMS Instantaneous Fields of View Projected onto Earth's Surface. The right portion (samples 1-18) of two consecutive scans are shown, and a portion of a scan from the previous orbit is also shown to illustrate the overlap of consecutive orbits at the equator. The higher orbit of the Meteor-3 Spacecraft results in more overlap than was present for Nimbus-7 TOMS.

Meteor–3 was launched in an orbit with an 82.5-degree inclination. The orbit precessed relative to Earth-Sun line with a period of 212 days, unlike Nimbus–7, which had a Sun-synchronous orbit. Because of the precession of the orbit, the local equator crossing time changed with the same period. During two periods within this cycle, the instrument was close to the terminator where ozone retrieval is difficult; consequently, during these periods, Level–3 ozone data have not been made available.

The ozone retrieval uses albedo determined as the ratio of the backscattered Earth radiance to the incident solar irradiance. This required periodic measurements of the solar irradiance. To measure the incident solar irradiance, the TOMS scanner could be positioned to view one of three ground aluminum diffuser plates housed in a carousel. The selected diffuser reflected sunlight into the instrument. The diffuser plate is the only component of the optical system not common to both the Earth radiance and the solar irradiance measurement. Only a change in the reflectivity of the diffuser plate can cause a change of the radiance/irradiance ratio with time. In principle, an accurate characterization of these changes will yield the correct variation of this ratio, and hence, an accurate long-term calibration of the instrument. The three diffuser plates were exposed at different rates, allowing calibration by examining the differences in degradation of diffuser reflectivity resulting from the different rates of exposure. A more detailed description of the instrument and its calibration appears in Section 3.

2.2 Algorithm

Retrieval of total ozone is based on a comparison between the measured normalized radiances and radiances derived by radiative transfer calculations for different ozone amounts and the conditions of the measurement. It is implemented by using radiative transfer calculations to generate a table of backscattered radiance as a function of total ozone, viewing geometry, surface pressure, surface reflectivity, and latitude. Given the computed radiances for the particular observing conditions, the total ozone value can be derived by interpolation in albedo as a function of ozone. It is also possible to reverse this process and use the tables to obtain the radiances that would be expected for a given column ozone and conditions of the measurement. The logarithm of the ratio of this calculated radiance to the measured radiance is the residue.

The reflecting surface is assumed to consist of two components, a surface component of lower reflectivity and a cloud component of higher reflectivity. By comparing the measured radiance at the ozone-insensitive 380 nm wavelength with that calculated for cloud and for ground reflection alone, the cloud fraction and the contribution from each level can be derived. Using this cloud fraction and the radiances measured at one pair of wavelengths, an initial ozone estimate is derived using the tables. This ozone estimate is then used to calculate the residues at all TOMS wavelengths except the longest. A correction to the initial ozone estimate is then derived from the residues at selected wavelengths. Applying this correction produces the Best Ozone value. The choice of wavelengths is based upon the optical path length of the measurement. Section 4 provides a full description of the algorithm.

2.3 Data Uncertainties

Uncertainties in the ozone values derived from the TOMS measurements have several sources: errors in the measurement of the radiances, errors in the values of input physical quantities obtained from laboratory measurements, errors in the parameterization of atmospheric properties used as input to the radiative transfer computations, and limitations in the way the computations represent the physical processes in the atmosphere. Each of these sources of uncertainty can be manifested in one or more of four ways: random error, an absolute error that is independent of time, a time-dependent drift, or a systematic error that will appear only under particular circumstances. For Meteor–3 TOMS total ozone, the absolute error is ± 3 percent, the random error is ± 3 percent and the drift for 40 months is less than ±1 percent, though somewhat higher at high latitudes. Because of algorithmic limitations at extreme measurement geometries associated with near terminator periods in the Meteor–3 orbital precession, only about half of the Meteor–3 TOMS Level–3 data is made available in the archive (Table 2.1). More detailed descriptions of the different sources of uncertainty and the extent to which each contributes to the overall uncertainty appear in Sections 3, 5, and 6. Section 3 discusses uncertainties due to errors in the characterization of the instrument sensitivity. Section 5 discusses other sources of random errors, absolute error, and drift, combining them with the instrument error to yield the overall estimates given above. Section 6 discusses errors that are limited in their scope to specific times, places, and physical conditions. Sections 5 and 6 also describe the remaining anomalies that have been identified in the Version 7 data, with a discussion of what is known of their origin.

Comparisons with Nimbus–7 TOMS and ground based measurements of total ozone indicate that the Meteor–3 TOMS data are consistent with these uncertainties during the Level–3 archive periods. Since the initial calibration of Meteor–3 has been adjusted to closely match the Nimbus–7 TOMS and the Nimbus–7 TOMS is known to agree well with ground based systems (McPeters et al., 1996), it is not surprising that the Meteor–3 TOMS agrees with both the Nimbus–7 TOMS and ground based measurements to better than 1 percent. The time dependent calibration of Meteor–3 TOMS is independent, however, and agrees with both of these systems to better than 1 percent over the entire instrument lifetime.

Data quality flags are provided with the derived ozone in the TOMS Ozone File (Level–2 data product). Only the data quality flag values of 0 and 10 are used to compute the averages provided on the CDTOMS (Level–3) product. Other flag values indicate retrieved ozone values that are of lower quality, allowing the users of Level–2 to decide whether or not they wish to accept such data for their applications.

Table 2.1. High Data Quality Periods for Meteor–3 TOMS. Level–3 data archive is restricted to these periods.

8/22/91	–	9/2/91
10/26/91	–	12/17/91
2/9/92	–	4/2/92
5/26/92	–	7/17/92
8/31/92	–	11/9/92
12/16/92	–	2/24/93
4/1/93	–	6/10/93
7/17/93	–	9/25/93
10/31/93	–	1/9/94
2/14/94	–	4/25/94
6/1/94	–	8/10/94
9/15/94	–	11/24/94

2.4 Archived Products

The Meteor–3 TOMS total ozone products are archived at the GSFC DAAC in Hierarchical Data Format (HDF). There are two kinds of total ozone products: the TOMS Ozone File or Level-2 Data Product, and the CDTOMS or Level-3 Data Product. The TOMS Ozone File contains detailed results of the TOMS ozone retrieval for each IFOV in time sequence. One file contains all the data processed for a single orbit. The CDTOMS contains daily averages of the retrieved ozone and effective surface reflectivity in a 1-degree latitude by 1.25-degree longitude grid. In areas of the globe where orbital overlap occurs, the view of a given grid cell closest to nadir is used, and only good quality retrievals are included in the average. Because of algorithmic limitations, the Level–3 data are archived only during periods when the local equator crossing time of the sunlit portion of the orbit is not too far from noon, or about half of the data (Table 2.1). Each CDTOMS file contains one daily TOMS map (0.4 megabyte/day). Detailed descriptions of these products are provided in Section 7.

Meteor–3 TOMS data will be put on CD–ROM for distribution by the GSFC DAAC. Daily average TOMS ozone in a uniform 1-degree latitude by 1.25-degree longitude grid over the entire globe will be available on a single CD covering the entire Meteor–3 TOMS lifetime.

3.0 INSTRUMENT

3.1 Description

The TOMS on board the Meteor–3 satellite measured incident solar radiation and backscattered ultraviolet sunlight. Total ozone was derived from these measurements. To map total ozone, TOMS instruments scan through the sub-satellite point in a direction perpendicular to the orbital plane. The Meteor–3 TOMS (M3/TOMS) instrument was originally the Nimbus–7 Engineering Model, and was built at the same time as the Nimbus–7 TOMS instrument. The optics of the two were, therefore, identical: a single, fixed monochromator, with exit slits at six near-UV wavelengths. The slit functions were triangular with a nominal 1-nm bandwidth. The order of individual measurements was determined by a chopper wheel. As it rotated, openings at different distances from the center of the wheel would pass over the exit slits, allowing measurements at the different wavelengths. The order was not one of monotonically increasing or decreasing wavelength; four samples at each wavelength were interleaved in a way designed to minimize the effect of scene changes on the ozone retrieval. The IFOV of the instrument was 3 degrees x 3 degrees. A mirror scanned perpendicular to the orbital plane in 3-degree steps from 51 degrees on the right side of spacecraft nadir to 51 degrees on the left (relative to direction of flight), for a total of 35 samples. At the end of the scan, the mirror would quickly return to the first position, not making measurements on the retrace. Eight seconds after the start of the previous scan, another would begin. Consecutive cross scans overlapped, creating a contiguous mapping of ozone. The higher altitude of M3/TOMS (1200 km compared to 996 km for N7/TOMS) meant greater overlap for M3/TOMS than for N7/TOMS.

The Meteor–3 orbit had an orbital inclination of 82.5 degrees. Unlike Nimbus–7, the orbit was not Sun-synchronous but had a precession period of 212 days. The first data were obtained on August 22, 1991, from an ascending (south-to-north) orbit that crossed the equator at 10:30 in the morning. As time passed, the ascending portion of the orbit precessed in a direction corresponding to progressively earlier times, first to the sunrise terminator, then through the night to the sunset terminator, across the afternoon through noon, returning 212 days later to 10:30 a.m. However, because the precession cycle is not equal to a year, the positions of the orbits relative to the terminator do not repeat exactly from one cycle to the next. As the position of the terminator relative to the pole will differ at the same phase of different cycles, the inclination of the orbit to the terminator will also differ, except for the noon and midnight orbits. Consider, for example, an orbit with a sunrise ascending node. At the equinox, the terminator will be at the pole, and the orbit will pass 7.5 degrees from it. At the solstice, the terminator is 23.5 degrees away, and an orbit with an 82.5 degrees inclination may pass between 16 degrees and 30 degrees from the point of the terminator nearest the pole, depending on the orientation of the orbit. During the periods when the ascending node was at night, data were taken during the descending portion of the orbit. This resulted in almost continuous global coverage.

In preparation for flight on Meteor–3, the instrument was refurbished and a number of improvements made. The diffraction grating was replaced, the mirrors were resurfaced, flight-qualified electronics were added, and a solid state data recorder replaced the tape recorder that had been used for Nimbus–7. Because of the high reliability of the solid state recorder, almost no data were lost during the three year mission. An IAM was added to allow the TOMS instrument, which had been designed to work with Nimbus satellites, to operate with Meteor–3. It converted the Meteor–3 power, commands, clock, telemetry, and data interfaces into a system compatible with TOMS. The most significant change in the instrument was the replacement of the single diffuser plate of Nimbus–7 with a three-diffuser system on Meteor–3 (Jaross et al., 1995) similar to that used on the Solar Mesosphere Explorer (Rottman et al., 1982). Aside from the change in the diffuser, the optics were identical to those described by Heath, et al. (1975) for Nimbus–7 TOMS.

Backscatter ultraviolet instruments measure the response to solar irradiance by deploying a ground aluminum diffuser plate to reflect sunlight into the instrument. Severe degradation of the Nimbus–7 diffuser plate was observed as time passed, and determining the resultant change of the instrument sensitivity with time proved to be one of the most difficult aspects of the instrument calibration (Cebula et al., 1988; Fleig et al., 1990, Herman et al., 1990; McPeters et al., 1993; Wellemeyer et al., 1996). The three-diffuser system aboard Meteor–3 reduced the exposure and degradation of the diffuser used for the solar measurements and allowed calibration through comparison of signals reflected off diffusers with different rates of exposure. The diffusers, designated cover, working, and reference, were arranged as the sides of an equilateral triangle and mounted on a carousel, so that a given diffuser could be rotated

into view on demand. The reference diffuser was normally exposed for one sequence every 106 days (half the period of orbital precession), the working diffuser for 6–8 sequences during that same period, and the cover diffuser was exposed for the remainder of the time, whether or not the solar flux was being measured. Comparison of the solar irradiance measurements from the different diffusers was used to infer that the degradation of the reference diffuser was negligible.

Solar measurements could be made only near the poles when the Sun was near the horizon, and within the 90-degree azimuthal field of view. As the equator crossing time of the orbit changed, the solar azimuth, and consequently the angle of incidence on the diffuser, would change as well. The diffuser's view of the Sun was obstructed over a large range of solar azimuth angles when the Sun was behind the instrument. Consequently, calibration was possible only during 55-day periods or about half the orbits.

The TOMS scanner had four operating modes determining data processing sequences and data formats:

1. Normal scan mode.
2. Single step mode.
3. View diffuser mode.
4. Stowed mode.

The primary operating mode of the TOMS was the normal scan mode. It was in this mode that the scanning mirror sampled the 35 scenes corresponding to the scanner view angles, measuring the backscattered Earth radiances used for deriving column ozone. In the single step mode, the scanner could be controlled directly by ground commands rather than carrying out an automatic sequence; however, this mode was never used. Solar irradiance measurements were made in the view diffuser mode. The scanner would move to the view diffuser position and stop. In-orbit wavelength and electronic monitoring occurred in the stowed mode. In the stowed position, the scan mirror is pointed into the instrument at a black surface. Wavelength monitoring is discussed in greater detail in Section 3.3.

Heath et al., (1978) describe the original TOMS instrument and its operation in greater detail. A detailed description of the TOMS adaptations for Meteor is provided by NASA (1993), and the prelaunch and postlaunch calibrations are described by Jaross et al., (1995).

3.2 Radiometric Calibration

Conceptually, the calibration of the TOMS measured Earth radiance and solar irradiance may be considered separately. The Earth radiance can be written as a function of the instrument counts in the following way:

$$I_m(t) = C_r k_r G_r f_{inst}(t) \tag{1}$$

where

$I_m(t)$	=	derived Earth radiance
C_r	=	counts detected in earth radiance mode
k_r	=	radiance calibration constant
G_r	=	gain range correction factor
f_{inst}	=	correction for instrument changes

The measured solar irradiance, F_m can be written as:

$$F_m(t) = C_i k_i G_i f_{inst}(t) / g\rho(t) \tag{2}$$

where

C_i = irradiance mode counts
k_i = irradiance calibration constant
G_i = gain range correction factor
f_{inst} = correction for instrument changes
$\rho(t)$ = solar diffuser plate reflectivity
g = relative angular correction for diffuser reflectivity

In practice, however, there is no attempt to accurately determine k_r or k_i separately, either their absolute value or time dependent changes. The primary quantity measured by TOMS and used to derive ozone is the normalized radiance, I_m/F_m. The advantage of this approach is that the spectrometer sensitivity changes affecting both the Earth and solar measurements (f_{inst}) cancel in the ratio.

The ratio becomes:

$$\frac{I_m}{F_m} = \frac{C_r}{C_i} K \frac{G_r}{G_i} g\rho(t) \tag{3}$$

where K is a combined calibration constant for TOMS normalized radiances referred to as the albedo calibration constant (Table 3.1). Radiance and irradiance measurements are generally made in different gain ranges, but evidence indicates that G has been properly characterized (see Section 3.6). The initial absolute TOMS calibration involves knowledge of the quantity $k_r g/k_i$. Since the instrument changes affecting both the Earth and solar measurements cancel in the ratio, the quantity critical to the time-dependent calibration of the normalized radiance is the diffuser plate reflectivity, $\rho(t)$. The angular dependence, g, is primarily required to correct for the diffuser Bi-directional Reflectivity Distribution Function (BRDF), but also contains the small correction due to light scattered from the instrument.

Table 3.1. Meteor–3 TOMS Albedo Calibration Constants and Gain Range Ratios.

Vacuum Wavelength (nm)	Albedo Cal Constant ($ster^{-1}$)	Adjustment Factor (ratio)
312.35	0.2389	0.940
317.40	0.2421	0.957
331.13	0.2479	0.945
339.73	0.2501	0.945
360.00	0.2529	0.951
380.16	0.2571	0.935
Gain Range Ratios		
Range 2/1	Range 3/2	Range 4/3
6.59	7.20	7.19

3.2.1 Absolute Calibration

In the Version 6 data set, the determination of the initial instrument calibration was based on the BRDF of the flight diffuser measured on the ground. This calibration is described in Jaross et al., 1995. In the Version 7 processing, however, the initial calibration is tied to that of Nimbus–7 TOMS. The normalization factors relative to the initial prelaunch calibration constants were determined by comparing nearly coincident measurements of the two instruments under similar viewing conditions.

For 380 nm, normalization was carried out by comparing near-nadir measurements with solar zenith angles between 20 and 40 degrees where both instruments viewed the same scene at close to the same time. Because of the

precession of the Meteor–3 orbit, there were only 5 periods of about 10 days each during which the Local Equator Crossing Time (LECT) was sufficiently close to that of Nimbus–7 that common scenes were viewed. At the A-pair wavelengths (312 and 331 nm), the same procedure was carried out, but with corrections for small differences in ozone and surface reflectivity.

The initial calibrations of the remaining wavelengths have also been adjusted in Version 7. The main motivation for this adjustment is algorithmic. Since different wavelengths are used to determine total ozone in different solar zenith angle regimes, it is imperative that the wavelength dependence of the initial calibration be consistent with the forward model calculation of the theoretical radiances used in the retrieval. Any inconsistencies can be identified through analysis of the residues (see Section 4.5 for further discussion of the residues). In cases where the A-triplet (313 nm, 331 nm, 380 nm) wavelengths are used to determine total ozone and effective reflectivity, adjusted residues can be computed for the other wavelengths (318 nm, 340 nm, 360 nm). These specifically characterize the inconsistency of these measured radiances with the total ozone and reflectivity derived using the A-triplet. Modal residues from the global population of A-triplet retrievals from the Meteor/Nimbus overlap data set were used to estimate the necessary adjustments (Table 3.1).

3.2.2 Time-Dependent Calibration

As discussed in the introduction to this section, the time-dependent calibration requires a correction for changes in the reflectivity of the solar diffuser plate. The Meteor–3 TOMS was equipped with a carousel with three diffusers that were exposed to the degrading effects of the Sun at different rates. The cover diffuser was exposed almost constantly, but the working diffuser was exposed weekly, and the reference diffuser was exposed only 11 times during the entire 3-year mission, each time in the same optimal viewing geometry. While the cover diffuser degraded quite rapidly, neither the working nor the reference diffuser degraded significantly during the life of the mission.

There is evidence from several sources that neither the working diffuser nor the reference diffuser degraded significantly. The ratio of solar fluxes derived from the cover diffuser to those derived from the working diffuser changes with time, indicating degradation of the cover diffuser. But the working diffuser measurements show no change with time relative to the reference diffuser measurements, in spite of the fact that the working diffuser was exposed approximately seven times as long as the reference diffuser. Also, the measurements of nadir radiances over ice described in Section 3.6 are consistent with the calibration derived assuming no diffuser degradation, and studies using the spectral discrimination technique give results consistent with no Meteor–3 diffuser degradation. Thus, $\rho(t)$ drops out of Equation 3 if only working or reference measurements are used, and the angular response, g, is the sole external characterization needed. Prelaunch measurement of the instrument angular response is described in Section 3.5.

The solar measurements were made near the northern or southern terminators when the back of the spacecraft and the TOMS solar diffuser carousel are exposed to the Sun. Because of the precessing Meteor–3 orbit there are periods of a month during which no valid solar measurements are made. This leads to a complication in the application of equation 3. Since C_r and C_i cannot be measured simultaneously, C_i must be characterized at the time at which C_r is measured. Fitting the solar flux measurements to solve this problem is simplified if the data are corrected for variations in sun/earth distance. Plots of this quantity for the working and reference diffusers are shown in Figure 3.1 normalized to the first solar measurement made using the reference diffuser. This quantity, which is equivalent to f_{inst} (Equation 2), has been fit with polynomials to provide a continuous characterization of C_i as a function of time from the solar measurements. For 360 nm, the fit was made to reference diffuser measurements. Working diffuser measurements suggest a dependence of the measured solar flux on the geometry of the measurement. These dependencies are seen as upward tails in the working diffuser measurements near the data gaps. The origin is not known, but possible goniometry or attitude determination problems are suspected because the tails occur where the diffuser angle of incidence is highest. Reference diffuser measurements were all made at normal incidence, and thus the time series is not affected. Because of the apparent change in chopper synchronization phase in May 1993, discussed in Section 3.8, separate fits were made to the data before and after this date, with a step discontinuity at the date of the change. A second-order polynomial was fit to the 360-nm reference diffuser measurements. For the other

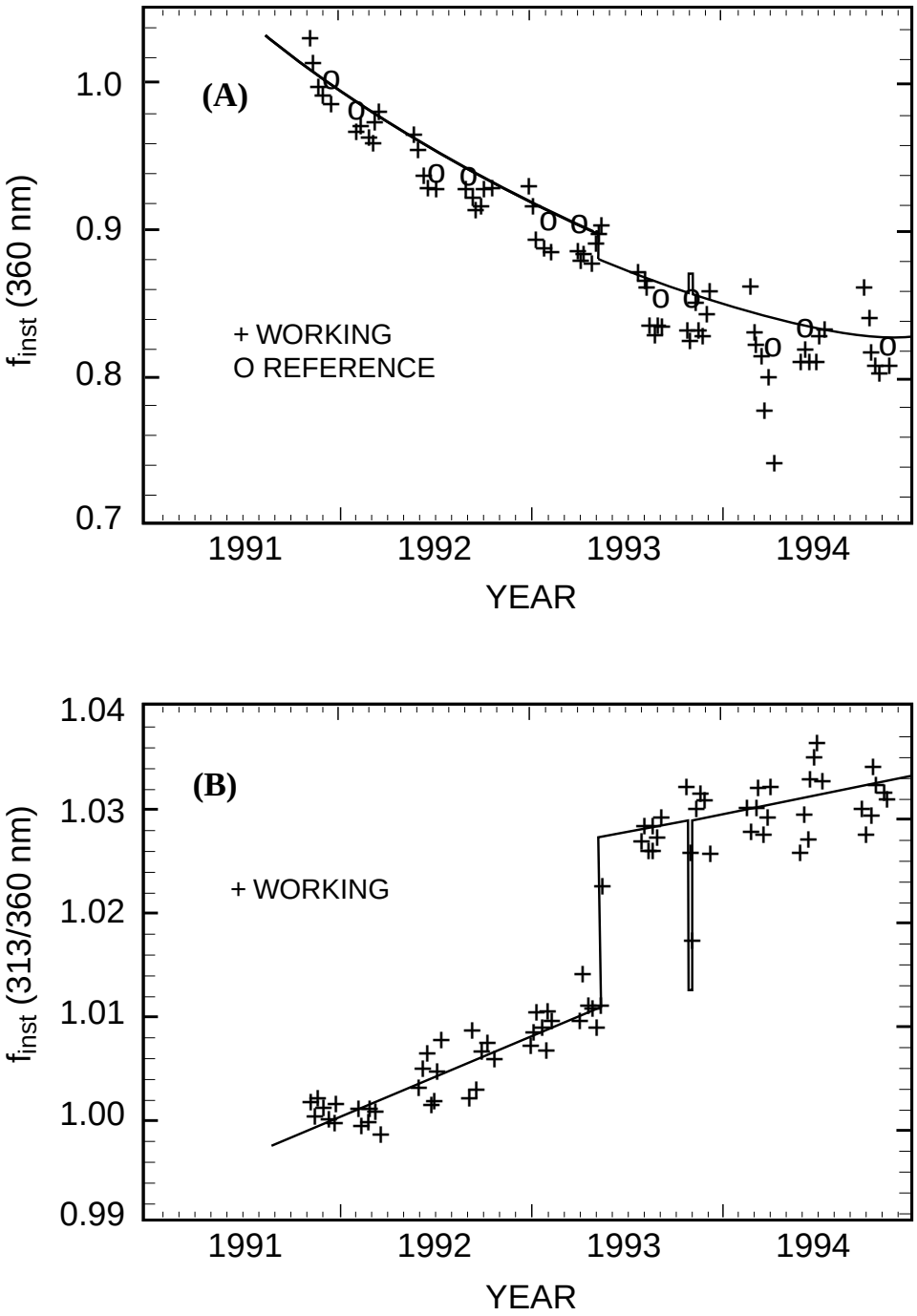

Figure 3.1. Estimated Change in TOMS Instrument Sensitivity Based on Solar Measurements Using the Working and Reference Diffusers. Fit characterizations used in the Version 7 processing are shown.

five wavelengths, ratios of the measured solar flux to the 360-nm value were used to fit the wavelength dependence. Because these ratios did not show a significant geometrical dependence, they were derived using working diffuser measurements. First order polynomial fits were used, with the periods before and after the chopper synchronization phase change treated separately. Samples of the various fits are shown in Figure 3.1.

3.3 Wavelength Monitoring

The Meteor–3 TOMS prelaunch wavelength calibration was determined prior to instrument assembly using only the slit plate, grating, and main mirror. The positions of back-illuminated white light images of the exit slits were compared to the positions of the spectral-line images of Hg, Zn, and Cd sources located at the entrance slit. Table 3.1 presents the derived wavelengths and associated constants.

Following this laboratory calibration, an on-board wavelength monitor tracked changes in the wavelength scale, both before launch and in orbit. Change might be produced by excessive temperature differentials or mechanical displacement of the wavelength-determining components resulting from shock or vibration. Scans of an internal mercury-argon lamp for in-flight monitoring of the wavelength selection were executed every 13th orbit during nighttime. The wavelength calibration was monitored by observing four wavelength bands near the center and in the wings of the 296.7-nm Hg line. Relative changes in the signal level would indicate wavelength shifts. There is no evidence of any prelaunch wavelength drift. Measurements after launch suggest variations of ±0.025 nm associated with changes in the instrument temperature as the orbit precessed and the time of day changed. These wavelength shifts would affect the derived ozone by only a quarter of a percent at mid and high latitude, an insignificant contribution to the overall uncertainty. Wavelength monitoring became more difficult in 1992, when occasional 0.02-nm changes began to appear, coinciding with shifts in lamp output. However, no changes in solar signal, which would be expected if the wavelength band actually shifted along the solar spectrum, were seen. The 0.02-nm changes are believed to be due to changes in other components of the instrument rather than to a change in the wavelength scale. Overall, the wavelength selection of the instrument is believed to have shifted by no more than 0.04 nm since launch. The largest impact of this shift on derived ozone occurs in the A-triplet, and is less than 1 percent.

3.4 Attitude Determination

On-board readings of the attitude control system indicated that little attitude adjustment of Meteor–3 was necessary. Comparisons carried out by the Hydromet CAO of infrared images from a high resolution instrument on-board Meteor–3 with locations inferred from the on-board sensors indicated small maximum periodic attitude errors of 0.34 degrees in roll, 0.55 degrees in pitch, and 0.30 degrees in yaw. However, study of the scan angle dependence in observations over Antarctica has indicated a yaw error. Asymmetry in the derived surface reflectivity as the instrument approached the terminator in a 1200 GMT or 2400 GMT LECT led to the conclusion that a constant 1.4-degrees yaw error was present in the previously processed data. All of the angles used and reported in the Version 7 processing have been recomputed based on this conclusion.

3.5 Angular Dependence of Diffuser Reflectivity

Because the Meteor–3 satellite did not have a Sun-synchronous orbit, the angle of incidence of the solar irradiance on the diffuser plate at the time when the solar measurements were taken changed with the time of day of the orbit. This angle would also change as the satellite orbited the Earth during a solar irradiance measurement. To accurately derive the relative solar irradiance therefore requires that the angular or goniometric dependence of the diffuser reflectivity be known.

The prelaunch goniometric calibration was performed by the instrument manufacturer. A monochromator with a 200-W quartz halogen lamp was used as a 2-nm bandwidth source at the TOMS wavelengths. A target assembly held the diffuser carousel in the same configuration relative to the source as in the instrument. This assembly could be rotated about two axes to change the direction of the incident light in the same way that would occur in flight. Measurements were made for all three diffusers for the full range of incidence angles that were anticipated in flight. From these measurements, the diffuser reflectivity and its angular dependence were derived. The non-smooth behavior of the working diffuser measurements shown in Figure 3.1(a) suggests errors in the prelaunch goniometric calibration. The upward tails seen in the figure are probably the result of characterization errors at the highest incidence angles. Since

the ozone determination is based on comparison of pairs and triplets of wavelengths, only wavelength dependent errors in the goniometric calibration will significantly affect the ozone determination. After goniometric correction, variations of relative spectral irradiance response observed in flight are within 0.5 percent (see Figure 3.1(b)).

3.6 Gain

The current from the Photo-Multiplier Tube (PMT) was fed to four electronic amplifiers in parallel, each of which operated in a separate gain range. The choice of which amplifier output was recorded for each measurement was based upon the signal level. Thus, knowledge of the gain ratios between ranges represents part of the determination of instrument linearity, and the stability of the gain ratios can affect the time-dependent calibration of the normalized radiance (Equation 3). The three ratios were determined electronically prior to launch. The value of the ratios directly affects the ozone retrieval because the solar calibration takes place in only the least sensitive range, and earth measurements occur in all ranges.

In the postlaunch phase, gain was monitored by sending two signals in each gain range from a precision current generator to the system once each day, immediately following the wavelength calibration. The instrument and spacecraft then process these test signals in the same way as the data from the PMT. The gain ratios were also studied by observing the signal change when viewing Antarctic ice. The cosine effect on the Earth-view signal as the instrument scene approaches the day/night terminator means that the signal passes through all four ranges in a short period of time. Requiring that the time dependence of the instrument signal was smooth yielded the gain range ratios. On the basis of these measurements, the range 3 to range 4 gain ratio was adjusted downward by just over 1 percent relative to prelaunch values. However, there was no evidence that the gain range ratios changed during flight (Table 3.1).

3.7 Thermal Correction

Changes in spectrometer sensitivity can be monitored through measurements of the reflectivity of ice surfaces, which are stable over the long-term to better than 1-2 percent (Jaross and Krueger, 1993). Most of this change arises from the process of measurement rather than from the variations in the actual reflectivity of the ice surfaces. One pattern of fluctuations in the radiances measured from ice as a function of time suggested a thermal sensitivity in the PMT. A linear fit was applied to the radiances as a function of time and temperature. Separate fits were applied to four distinct time intervals, in order to eliminate the effects of possible overall spectrometer change. A thermal sensitivity of -0.32±0.01 percent/°C was derived and applied as a correction to the radiances. This amounts to at most a 5-percent correction to radiances, 3 percent of which occurs in a 4-week period surrounding a terminator orbit. There is no evidence that the thermal dependence varies from wavelength to wavelength.

3.8 Chopper Wheel Problems

The operation of the TOMS chopper wheel is designed to be synchronized with the electronics such that the signal will be recorded at the time that the chopper opening is positioned over one of the exit slits. A telemetry flag indicates whether the chopper and electronics are properly synchronized. Starting in May 1993, this flag was indicating a loss of synchronization nearly all of the time. A decrease of about 4 percent in the solar signal provided direct evidence of synchronization problems, since such a decrease would occur if the chopper was not positioned directly over the slit when the electronics were recording. Although the data noise doubled, it was still small relative to the signal. This suggests that the relative phase of the chopper and the electronics was not varying significantly, even though they were not as originally designed. This quasi-synchronized condition could be treated as a change in sensitivity, and accurate ozone values could be retrieved by tracking the change in instrument sensitivity through the measured solar flux as described in Section 3.2 and Figure 3.1.

For brief periods since May 1993, generally lasting no longer than one orbit, the chopper phase would change so rapidly that no stable correction to the instrument calibration was possible. These periods tend to cluster at times of lowest spacecraft temperature, suggesting a connection with the viscosity of the lubricant in the chopper motor bearings. These data can be identified because retrievals using different wavelength pairs give inconsistent results. In most instances, these data are rejected and flagged by the algorithm (Section 4.6), but some affected data remain. This

is particularly true of the time period between May 20, 1993 and June 30, 1993. These errors can represent as much as 2 percent in ozone, specifically in the B-triplet used at higher optical path lengths.

4.0 ALGORITHM

The Meteor–3 TOMS algorithm is identical to the Nimbus–7 TOMS algorithm. This section (including equation numbers) is a duplication of the Nimbus–7 TOMS algorithm section (McPeters et al., 1996) except that the values in the tables are slightly different due to small differences in the band center wavelengths.

4.1 Theoretical Foundation

To interpret the radiance measurements made by the TOMS instrument requires an understanding of how the Earth's atmosphere scatters ultraviolet radiation as a function of solar zenith angle. Incoming solar radiation undergoes absorption and scattering in the atmosphere by atmospheric constituents such as ozone and aerosols and by Rayleigh scattering. Radiation that penetrates to the troposphere is scattered by clouds and aerosols, and radiation that reaches the ground is scattered by surfaces of widely varying reflectivity.

The backscattered radiance at a given wavelength depends, in principle, upon the entire ozone profile from the top of the atmosphere to the surface. The two shortest wavelengths used in the TOMS ozone measurements were selected because they are absorbed by ozone. At these wavelengths, absorption by other atmospheric components is negligible compared to that by ozone.

At wavelengths longer than approximately 310 nm, however, the backscattered radiance consists primarily of solar radiation that penetrates the stratosphere and is reflected back by the dense tropospheric air, clouds, aerosols, and the Earth's surface. The intensity is determined primarily by the total optical depth above the scattering layer in the troposphere. The amount of ozone below the scattering layer is small and can be estimated with sufficient accuracy to permit derivation of total column ozone. Because most of the ozone is in the stratosphere, the principal effect of atmospheric ozone at these wavelengths is to attenuate both the solar flux going to the troposphere and the component reflected back to the satellite.

Derivation of atmospheric ozone content from measurements of the backscattered radiances requires a treatment of the reflection from the Earth's surface and of the scattering by clouds and other aerosols. These processes are not isotropic; the amount of light scattered or reflected from a given scene to the satellite depends on both the solar zenith angle and view angle, the angle between the scene and the nadir as seen at the satellite.

The algorithm used for previous releases based its calculation of reflectivity on the treatment of Dave (1978), who represented the contribution of clouds and aerosols to the backscattered intensity by assuming that radiation is reflected from a particular pressure level called the "scene pressure," with a Lambert-equivalent "scene reflectivity" R. When this method was applied, at the non-ozone-absorbing wavelengths the resulting reflectivity exhibited a wavelength dependence correlated with partially clouded scenes. To remove this wavelength dependence, a new treatment has been developed, based on a simple physical model that assumes two separate reflecting surfaces, one representing the ground and the other representing clouds. The fractional contribution of each to the reflectivity is obtained by comparing the measured radiances with the values calculated for pure ground and pure cloud origin.

The calculation of radiances at each pressure level follows the formulation of Dave (1964). A spherical correction for the incident beam has been incorporated, and Version 7 treats molecular anisotropy (Ahmad and Bhartia, 1995) Consider an atmosphere bounded below by a Lambertian reflecting surface of reflectivity R. The backscattered radiance emerging from the top of the atmosphere as seen by a TOMS instrument, I_m, is the sum of purely atmospheric backscatter I_a, and reflection of the incident radiation from the reflecting surface I_s,

$$I_m(\lambda, \theta, \theta_0, \Omega, P_0, R) = I_a(\lambda, \theta, \theta_0, \phi, \Omega, P_0) + I_s(\lambda, \theta, \theta_0, \phi, \Omega, P_0, R) \quad (9)$$

where

- λ = wavelength
- θ = satellite zenith angle, as seen from the ground
- θ_0 = solar zenith angle

ϕ = azimuth angle
Ω = column ozone amount
P_0 = pressure at the reflecting surface
R = effective reflectivity at the reflecting surface

The surface reflection term can be expressed as follows:

where

$$I_s(\lambda,\theta,\theta_0,\Omega,P_0,R) = \frac{RT(\lambda,\theta,\theta_0,\Omega,P_0)}{1-RS_b(\lambda,\Omega,P_0)} \tag{10}$$

$$T(\lambda,\theta,\theta_0,\Omega,P_0) = I_d(\lambda,\theta,\theta_0,\Omega,P_0)\, f(\lambda,\theta,\Omega,P_0) \tag{11}$$

where

S_b = fraction of radiation reflected from surface that atmosphere reflects back to surface
I_d = total amount of direct and diffuse radiation reaching surface at P_0
f = fraction of radiation reflected toward satellite in direction θ that reaches satellite,

and the other symbols have the same meaning as before. The denominator of Equation 10 accounts for multiple reflections between the ground and the atmosphere.

The intensity of radiation as it passes through a region where it is absorbed and scattered can be described in general terms as having a dependence $I \propto \exp(-\tau)$. For a simplified case, where all processes can be treated as absorption, the optical depth τ depends on the number of absorbers *n* in a column and the absorption efficiency α of the absorbers; that is, $I \propto \exp(-n\alpha)$. The column number should thus scale approximately as -log I. The ozone algorithm therefore uses ratio of radiance to irradiance in the form of the N-value, defined as follows:

$$N = -100 \log_{10}\left(\frac{I}{F}\right) \tag{12}$$

The N-value provides a unit for backscattered radiance that has a scaling comparable to the column ozone; the factor of 100 is to produce a convenient numerical range.

The basic approach of the algorithm is to use a radiative transfer model to calculate the N-values that should be measured for different ozone amounts, given the location of the measurement, viewing conditions, and surface properties, and then to find the column ozone that yields the measured N-values. In practical application, rather than calculate N-values separately for each scene, detailed calculations are performed for a grid of total column ozone amounts, vertical distributions of ozone, solar and satellite zenith angles, and two choices of pressure at the reflecting surface. The calculated N-value for a given scene is then obtained by interpolation in this grid of theoretical N-values.

The ozone derivation is a two-step process. In the first step, an initial estimate is derived using the difference between N-values at a *pair* of wavelengths; one wavelength is significantly absorbed by ozone, and the other is insensitive to ozone. Use of a difference provides a retrieval insensitive to wavelength-independent errors, in particular, any in the zero-point calibration of the instrument. In deriving the initial estimate, the same pair is always used.

In the second step, N-values are calculated using this ozone estimate. In general, these calculated values will not equal the measured N-values. The differences, in the sense $N_{meas}-N_{calc}$, are called the *residues*. Using the residues at a properly chosen *triplet* of wavelengths, it is possible to simultaneously solve for a correction to the original ozone estimate and for an additional contribution to the radiances that is linear with wavelength, arising primarily from wavelength dependence in the surface reflectivity but also possibly originating in the instrument calibration. The triplet consists of two pair wavelengths, as described above, plus 380 nm, which is insensitive to ozone. The pair

wavelengths used are those most sensitive to ozone at the optical path length of the measurement. The separation of the 380-nm wavelength from the pair wavelengths is far larger than the separation between the pairs; thus, the 380-nm measurement provides a long baseline for deriving wavelength dependence. This process may be iterated, using the results of the first triplet calculation as the new initial estimate. Table 4.1 lists the wavelengths of the pairs and triplets.

Table 4.1. Pair/Triplet Wavelengths

Pair/Triplet Designation	Ozone Sensitive Wavelength (nm)	Ozone Insensitive Wavelength (nm)	Reflectivity Wavelength (nm)	Range of Application (optical path s)
A	312.3	331.1	380.0	$1 \geq s$
B	317.4	331.1	380.0	$3 \geq s > 1$
B′	317.4	339.7	not used	validation only
C	331.1	339.7	380.0	$s > 3$

4.2 Calculation of Radiances

To carry out the calculation described in Section 4.1 requires the following information:

- Ozone absorption coefficients as a function of temperature for the wavelengths in the TOMS bandpasses.
- Atmospheric Rayleigh scattering coefficients.
- Climatological temperature profiles.
- Climatological ozone profiles.
- Solar zenith angle.
- Satellite zenith angle at the IFOV.
- Angle between the solar vector and the TOMS scan plane at the IFOV.
- Pressure at the reflecting surface.

Because of the its finite bandwidth, TOMS does not measure a monochromatic radiance. For comparison with the TOMS measurements, radiances are calculated at approximately 0.05-nm intervals across each of the TOMS slits, using the appropriate absorption coefficient and temperature dependence (Paur and Bass, 1985) for each wavelength. The I/F for the entire band, $A(\lambda_0)$, is then given by the following expression:

$$A(\lambda_0) = \int A(\lambda)F(\lambda)S(\lambda)d\lambda / \int F(\lambda)S(\lambda)d\lambda \qquad (13)$$

where

$A(\lambda) = \frac{I(\lambda)}{F(\lambda)}$ at wavelength λ,
$F(\lambda)$ = solar flux at wavelength λ,
$I(\lambda)$ = earth radiance at wavelength λ, and
$S(\lambda)$ = Instrument response function at wavelength λ.

The wavelength dependence of the solar flux is based on SOLSTICE measurements (Woods et al., 1996). This detailed calculation replaces the effective absorption coefficients used in Version 6.

Table 4.2 shows effective absorption coefficients for the Meteor–3 TOMS wavelengths. As discussed above, effective absorption coefficients are not used in the Version 7 algorithm. The same method of calculation was used as in Version 6, integrating the monochromatic laboratory values over the TOMS bandpass for the following conditions: a mid-latitude profile for Ω = 350, a path length of 2.5, and a wavelength-independent solar flux. These effective absorption coefficients are given in Table 4.2. Because the effective absorption coefficient depends on the ozone

profile, optical path length, and solar flux spectrum, the Version 7 technique of calculating I/F at individual wavelengths and then integrating over the TOMS bandpass eliminates the imprecision arising from using one set of effective absorption coefficients, derived for a particular set of conditions, for all calculations. Table 4.2 also contains the Rayleigh scattering coefficients and the regression equations used for the temperature dependence of the ozone coefficients. The values shown in the table are purely to illustrate the magnitude of the change; they have not been used in the algorithm.

Table 4.2. Effective Absorption and Scattering Coefficients

Vacuum Wavelength (nm)	Effective Ozone Absorption Coefficient (atm-cm^{-1}) at 0˚C (C_0)	Temperature Dependence Coefficients		Rayleigh Scattering Coefficient (atm^{-1})
		C_1	C_2	
312.35	1.9000	5.507×10^{-3}	2.922×10^{-5}	1.0220
317.40	0.9915	3.167×10^{-3}	1.768×10^{-5}	0.9543
331.13	0.1703	7.117×10^{-4}	4.199×10^{-6}	0.7967
339.73	0.0390	3.938×10^{-4}	2.816×10^{-6}	0.7145
360.00	$< 10^{-8}$	–	–	0.5597
380.16	$< 10^{-8}$	–	–	0.4458
Correction to ozone absorption for temperature: Ozone absorption = $C_0 + C_1T + C_2T_2$ (where T is in degrees C)				

Ozone and temperature profiles were constructed using a climatology based on SBUV measurements above 15 km and on balloon ozonesonde measurements (Klenk et al., 1983) for lower altitudes. Each standard profile represents a yearly average for a given total ozone and latitude. Profiles have been constructed for three latitude bands: low latitude (15 degrees), mid-latitude (45 degrees), and high latitude (75 degrees). There are 6 profiles at low latitudes and 10 profiles each at middle and high latitudes, for a total of 26. These profiles cover a range of 225–475 D.Us. for low latitudes and 125–575 for middle and high latitudes, in steps of 50 D.Us. The profiles are given in Appendix A.

To use the new Version 7 ozone profile weighting scheme for high path lengths, outlined in Section 2.2, it was necessary to extend the standard profiles beyond the available climatology. To minimize the use of extrapolation in this process, profile shapes were derived by applying a Principal Component Analysis to a separate ozone profile climatology derived from SAGE II and balloon measurements (Chu et al., 1989) to derive Empirical Orthogonal Functions (EOFs). The EOFs corresponding to the two largest eigenvalues represented more than 90 percent of the variance. The EOF with the greatest contribution to the variance was associated with variation in total ozone. The second most important EOF was associated with the height of the ozone maximum and correlated well with latitude, showing a lower maximum at higher latitude. This correlation was used as the basis for lowering the heights of the ozone maxima at high latitudes and raising them in the tropics when extending the original climatology to represent the more extreme profile shapes (Wellemeyer et al., 1996).

Given the wavelength, total ozone and ozone profile, surface pressure, satellite zenith angle at the field of view, and solar zenith angle, the quantities I_m, I_a, T, and S_b of Equations 9 and 10 can then be calculated at the six TOMS wavelengths. For the tables used in the algorithm, these terms are computed at the TOMS wavelengths for all 26 standard profiles and two reflecting surface pressure levels (1.0 atm and 0.4 atm). For each of these cases, I_m, I_a, T are calculated for ten choices of solar zenith angle from 0–88 degrees, spaced with a coarser grid at lower zenith angles and a finer grid for higher zenith angles, and for six choices of satellite zenith angle, five equally spaced from 0–60 degrees and one at 70 degrees. In Version 6, the tables extended only to a satellite zenith angle of 63.33 degrees. The fraction of reflected radiation scattered back to the surface, S_b, does not depend on solar or satellite zenith angle.

4.3 Surface Reflection

To calculate the radiances for deriving ozone from a given measurement requires that the height and reflectivity of the reflecting surface be known. The TOMS algorithm assumes that reflected radiation can come from two levels, ground and cloud. The average ground terrain heights are from the National Oceanic and Atmospheric Administration (NOAA) National Meteorological Center (NMC), provided in km for a 0.5-degree x 0.5-degree latitude and longitude grid, a finer resolution than the 2.5-degree x 2.5-degree grid used for Version 6. These heights are converted to units of pressure using a U.S. Standard Atmosphere (ESSA, 1966) and interpolated to the TOMS IFOVs to establish the pressure at the Earth's surface. Probabilities of snow/ice cover from around the globe are collected by the Air Force Global Weather Center and mapped on a polar stereographic projection. These data have been averaged to provide a monthly snow/ice climatology mapped onto a 1-degree x 1-degree latitude and longitude grid and used to determine the presence or absence of snow in the TOMS IFOV. If the probability is 50 percent or greater, snow/ice is assumed to be present. For cloud heights, a climatology based upon the International Satellite Cloud Climatology Project (ISCCP) data set is used. It consists of the climatological monthly averages over a 0.5 x 0.5-degree latitude-longitude grid. This climatology replaces the purely latitude-based climatology derived from Temperature-Humidity Infrared Radiometer (THIR) measurements used for Version 6, which placed the cloud layer at higher altitude closer to the equator. In particular, the ISSCP-based climatology better represents the low marine stratus over oceans and continental west coasts.

Reflectivity is determined from the measurements at 380 nm. For a given TOMS measurement, the first step is to determine calculated radiances at 380 nm for reflection off the ground and reflection from cloud, based on the tables of calculated 380-nm radiances. For reflection from the ground, the terrain height pressure is used, and the reflectivity is assumed to be 0.08, unless snow/ice is present, in which case 0.5 is used. For cloud radiances, a pressure corresponding to the cloud height from the ISCCP-based climatology is used, and the reflectivity is assumed to be 0.80. The ground and cloud radiances are then compared with the measured radiance. If $I_{ground} \leq I_{measured} \leq I_{cloud}$, and snow/ice is assumed not to be present, an effective cloud fraction *f* is derived using

$$f = \frac{I_{measured} - I_{ground}}{I_{cloud} - I_{ground}} \tag{14}$$

If snow/ice is assumed to be present, then the value of *f* is divided by 2, based on the assumption that there is a 50-50 chance that the high reflectivity arises from cloud. The decrease in *f* means that there is a smaller contribution from cloud and a higher contribution from ground with a high reflectivity off snow and ice. Equation 14 is solved for a revised value of I_{ground}, and the ground reflectivity is calculated from Equation 10. For the ozone retrieval, the calculated radiances are determined assuming that a fraction *f* of the reflected radiance comes from cloud with reflectivity 0.80, and a fraction *1-f* from the ground, with reflectivity 0.08 when snow/ice is absent and with the recalculated reflectivity when snow/ice is present. An effective reflectivity is derived from the cloud fraction using the following expression:

$$R = R_g(1 - f) + R_c f \tag{15}$$

where R_g is 0.08 when snow/ice cover is assumed absent and has the recalculated value when it is assumed present. This reflectivity is included in the TOMS data products but plays no role in the retrieval.

If the measured radiance is less than the ground radiance, then the radiation is considered to be entirely from surface terrain with a reflectivity less than 0.08. Equations 9 and 10 can be combined to yield:

$$R = \frac{I - I_a}{T - S_b(I - I_a)} \tag{16}$$

The ground reflectivity can be derived using an I_a obtained assuming ground conditions. Similarly, if the measured radiance is greater than the cloud radiance, when snow/ice are absent, the reflected radiance is assumed to be entirely

from cloud with reflectivity greater than 0.80, and an I_a derived using the cloud conditions is used in Equation 16 to derive the effective reflectivity. If snow/ice are present, the cloud and ground are assumed to contribute equally to I_m at 380 nm. Equation 16 can then be used to calculate new values of both ground and cloud reflectivities from these radiances. Radiances at the shorter wavelengths are calculated using these reflectivities and a value of 0.5 for *f*.

4.4 Initial B-Pair Estimate

The initial ozone is calculated by a modification of the Version 6 method, using the B-pair, which provides good ozone values over the largest range of conditions of any of the pairs.

The first step is to calculate radiances for the conditions of the measurement—geometry, latitude, cloud and terrain height, and cloud fraction. For each ozone value in the table, radiances are calculated for the 1.0 atm and 0.4 atm levels, using ground reflectivity and the values of I_a, T, and S_b from the tables for the geometry of the measurement and a single ozone profile—the low latitude profile for measurements at latitudes 15 degrees and lower, the mid latitude profile for 15 degrees < latitude ≤ 60 degrees, and the high latitude profile at latitudes higher than 60 degrees. These radiances are then corrected for rotational Raman scattering (the Ring effect). The correction factors, based on the results of Joiner et al., (1995), are shown in Table 4.3. They were computed using a solar zenith angle of 45 degrees and a nadir scan. The dependences on solar and scan angles, which are small under most conditions, are neglected. Two sets were calculated, one at 1 atm and the assumed 8 percent ground reflectivity for use with the 1-atm radiance tables and the other at 0.4 atm and the assumed 80 percent cloud reflectivity for use with the 0.4-atm tables. This correction, new for Version 7, greatly reduces the biases that had been seen between ozone values derived from different pairs in the Version 6 retrievals.

Table 4.3. Rotational Raman Scattering Corrections

	Radiance Correction (%)	
Actual Wavelength (nm)	Pressure = 1.0 atm Reflectivity = 8%	Pressure = 0.4 atm Reflectivity = 80%
312.35	0.33	0.20
317.40	–0.80	–0.44
331.13	0.19	0.10
339.73	–0.15	–0.08
360.00	–0.88	–0.39
380.16	0.26	0.11

The ground radiance is then derived by interpolating between values for the two pressures to derive the radiance for the pressure at the terrain height from the grid. A similar process is carried out for both pressures using cloud reflectivity, and the cloud radiance is derived by linear interpolation for the pressure level at the height given by the ISCCP cloud height climatology. Finally, the appropriate fractions of ground and cloud radiances, determined as described in Section 4.3, are added to yield I/F for all ozone values. These results are then converted to N-values.

The next step is to compare the measured radiance with the calculated radiance. The two tabulated ozone values whose calculated B-pair N-value differences bracket the measured N-value difference are identified in the table. A climatological ozone amount below the terrain pressure level is subtracted from these two bracketing table ozone values, and the initial ozone estimate is derived by linearly interpolating between the two resultant values, using the measured N-value and the two calculated N-values.

4.5 Best Ozone

Once an initial estimate of ozone has been obtained, it is used to calculate N-values at all TOMS wavelengths in the way described in Section 4.2, applying the rotational Raman scattering correction described in Section 4.4. N-values are calculated for each measurement, using one profile or two, depending upon the latitude. For latitude ≤ 15 degrees, only the low latitude profiles are used, for 15 degrees< latitudes ≤ 45 degrees, one set each is calculated using low and middle latitude profiles, for 45 degrees< latitudes < 75 degrees, N-values are calculated using middle and high

latitude profiles; and for latitude ≥ 75 degrees, only N-values for high latitude profiles are calculated. Values of dN/ dΩ are calculated, as well.

In general, these calculated N-values will not equal the measured N-values. In the derivation of the initial ozone estimate, reflectivity is assumed to be independent of wavelength, but for some surface conditions, such as sea glint, desert dust, or ice, the reflectivity will be wavelength dependent. In addition, residual errors in the instrument calibration can produce a wavelength dependent artifact in the measured N-value. Because of these effects on the spectrum of backscattered radiation and because of the simplifications used in its derivation, the initial ozone estimate will not be equal to the true ozone value. This error in ozone will also contribute to the discrepancy between the measured N-value N_m and the value N_0 calculated from the initial ozone estimate. The initial ozone estimate should, however, be sufficiently close to the true value to derive a correction using a first order Taylor expansion in the difference. The wavelength-dependent contribution from factors other than ozone, such as reflectivity and residual errors in the instrument characterization, is assumed to be a linear function of wavelength, a + bλ. Then,

$$N_m = N_0 + (\Omega - \Omega_0)\left(\frac{dN}{d\Omega}\right)_0 + a + b\lambda. \tag{17}$$

Let

$r_\lambda = (N_m - N_0)_\lambda$ be the residue at wavelength λ, and

$s_\lambda = \left(\frac{dN}{d\Omega}\right)_\lambda$ be the sensitivity at wavelength λ.

Equation 17 becomes:

$$r_\lambda = s_\lambda(\Omega - \Omega_0) + a + b\lambda. \tag{18}$$

The radiation at 380 nm is insensitive to ozone, and therefore $s_{380} = 0$. Further, since the reflectivity was derived at 380 nm, the residue is zero at that wavelength. Substituting into Equation 18 and solving yields:

$$a = -380b \tag{19}$$

and therefore, for the ozone-sensitive wavelengths,

$$r_\lambda = s_\lambda(\Omega - \Omega_0) + b(\lambda - 380). \tag{20}$$

There are two unknowns, Ω and b. Let Δλ = λ-380. Using measurements at two wavelengths, labeled λ_1 and λ_2, it is possible to solve for Ω:

$$\Omega = \Omega_0 + \frac{r_1\Delta\lambda_2 - r_2\Delta\lambda_1}{s_1\Delta\lambda_2 - s_2\Delta\lambda_1} \tag{21}$$

Equation 21 is the form in which the algorithm applies the correction. Ozone values are derived for each of the two profiles selected.

Another form of this equation is:

$$\frac{\Delta\lambda_2}{\Delta\lambda_1} = \frac{r_1 - s_1(\Omega - \Omega_0)}{r_2 - s_2(\Omega - \Omega_0)} \tag{22}$$

This form illustrates how the correction is equivalent to assuming that the size of that part of the residual not arising from ozone error is linear with wavelength.

For retrievals at latitudes where two profiles are used, an ozone value appropriate to the latitude of the measurement is then derived from the ozone values for the two profiles, using an equation of the following form:

$$\Omega = (1 - f_{prof})\Omega_{lower} + f_{prof}\Omega_{higher} \tag{23}$$

where

Ω	=	best ozone,
Ω_{lower}	=	ozone retrieved using lower latitude profile,
Ω_{higher}	=	ozone retrieved using higher latitude profile, and
f_{prof}	=	weight given to higher latitude profile.

Thus, f_{prof} will be 0 if only the lower latitude profile is selected, 1 if only the higher latitude profile is selected, and in between for a combination of the two profiles. The choice of pairs and f_{prof} depends upon the optical path length $\Omega_0(\sec\theta_0 + \sec\theta)$, in atm-cm.

For path lengths less than 1.5, a value of f_{prof} obtained by simple linear interpolation in latitude,

$$f_{prof} = \frac{|latitude| - |latitude|_{lower}}{|latitude|_{higher} - |latitude|_{lower}} \tag{24}$$

is used for latitudes between 15 and 75 degrees using the two profiles appropriate to the latitude. The low latitude profile alone is used from the equator to 15 degrees, and the high latitude profile alone is used from 75 degrees to the pole. For a path length less than or equal to 1.0, the A-triplet wavelengths are used in Equation 21; for a path length greater than 1 and no greater than 1.5, the B-triplet is used with the same latitude interpolation.

For longer path lengths, a different treatment is used for latitude interpolation. The basic principle is to require consistency between two triplets. For an arbitrary value of f_{prof}, the two triplets will give different ozone values. The value of f_{prof} is determined by finding the factor that yields the same ozone value for both triplets. For path lengths greater than 1.5 but no greater than 3, the B-triplet is used for the retrieval, and the profile is determined by requiring the A-triplet to be consistent, and for path lengths greater than 3, the C-triplet is used for the retrieval and a consistent B-triplet required. If the value derived using the low and middle latitudes is greater than one, the middle and high latitudes profiles are used; similarly if using the middle and high latitudes gives a value less than zero, the low and middle latitudes are used. The minimum value accepted using the two lower-latitude profiles is –0.5, and the maximum accepted using the two higher is 1.5, to avoid extreme extrapolation in either case.

The implementation of this approach uses residues. First, ozone values Ω_1 are calculated using Equation 21 for the two appropriate latitude profiles and interpolation in latitude as specified by Equation 24. The B-triplet is used for path lengths below 3, and the C-triplet is used for higher path lengths. Sensitivities are also calculated using latitude interpolation between the sensitivities for the standard profiles.

Rather than computing the radiances for the new set of ozone values Ω_1 to obtain the residues r_1 for this new ozone value, the following equation is used to adjust the residues for the change in ozone:

$$r_i = r_0 - s_i(\Omega_i - \Omega_0), \tag{25}$$

with *i* equal to 1. By Equation 20,

$$r_{1,\lambda} = b(\lambda - 380), \tag{26}$$

for the wavelengths used in the triplet ozone determination. For other wavelengths λ, the *triplet residue* can be defined as the difference between the residue at that wavelength and the value that would fall on the line defined by

$$r_{trip} = r - \frac{\lambda - 380}{\lambda' - 380} r', \tag{27}$$

where λ' is a wavelength used in the derivation of Ω_1 and r' is the value of r_1 at that wavelength. If two triplets differ only in one wavelength, a consistent result requires that the residues for all wavelengths in both triplets fall on the same line. For example, when ozone is calculated using the B-triplet, a consistent A-triplet ozone value requires that the triplet residue at 312 nm, which is used for the A-triplet but not for the B triplet, be zero; similarly, for B-triplet ozone to be consistent with ozone derived using the C-triplet, the 317 nm triplet residue must be zero. To find the profile that will yield consistency, the triplet residue for the appropriate wavelength is calculated for each of the two standard profiles. Then f_{prof} is set to be

$$f_{prof} = \frac{r_{trip}(lower)}{r_{trip}(lower) - r_{trip}(higher)} \tag{28}$$

where lower and higher refer to latitudes of the two profiles used. In most cases, the appropriate profile will be between the higher and lower latitude profiles, and the residues will be of opposite sign; thus the denominator represents a distance between the residues and the numerator a fraction of this distance. If, for example, the lower-latitude residue has a significantly larger absolute value, the value of f_{prof} is close to one; the profile chosen is close to the higher latitude profile. The value of f_{prof} derived from Equation 28 is then used to calculate a new ozone value Ω_2. Adjusted residues are calculated using Equation 25, and a new triplet residue is derived, using Equation 27. If this triplet residue is 0.10 or less in N-value units, then Ω_2 is adopted as the Best Ozone value; otherwise, the process is repeated, beginning with the derivation of residues for the new ozone value using Equation 25 with *i* equal to 2. This second result (Ω_3) is then accepted as Best Ozone. When the low- and mid-latitude profiles are used, if the derived value of f_{prof} is greater than 1, the process is repeated using the mid- and high-latitude profiles; similarly, if $f_{prof} < 0$ when using mid- and high-latitude profiles, the process is repeated using the low- and mid-latitude profiles. Finally, if the first derived Ω_{best} differs from the estimated value from the B-pair calculation by more than 50 D.Us., then the procedure starting with Equation 21 is repeated, using this initial Ω_{best} as the Ω_0. The result of this recalculation is adopted as Best Ozone. After a Best Ozone value has been accepted, residues are calculated from Equation 25 for each of the latitude profiles used, and final residues are derived by interpolating using f_{prof}.

The final step is to estimate the amount of the derived ozone that is beneath clouds. Estimates of the ozone amount under the cloud level pressure level are obtained for each of the two latitude profiles used to derive Best Ozone and the two tabulated ozone values on either side of the derived Best Ozone. The column ozone beneath cloud is then derived by interpolating in ozone and using f_{prof} to weight the latitudes. Finally, this ozone amount is multiplied by the cloud fraction f to derive the ozone in a particular field of view that is under cloud. The sensitivities are calculated from the sensitivities for the two profiles using the same weighting as for ozone.

4.6 Validity Checks

The algorithm contains several validity checks for maintaining data quality. Before measured radiances are accepted for use in ozone determination, the solar zenith angle, satellite attitude, and instrument status are checked to ensure the suitability of the radiances and other geophysical input to the algorithm. This section describes the quality checks performed to identify invalid and lower quality ozone values caused either by bad input data that passed preprocessing checks or by limitations of the ozone algorithm. It also explains the significance of the error flags that are set.

The principal tool used to investigate the validity and quality of a total ozone value is the set of residues. The residues measure how well radiances calculated based on the ozone derived using one set of wavelengths match the radiances measured at the other wavelengths. The usual significance of a large residue is that the atmospheric or surface conditions deviate significantly from those assumed in the algorithm, for example, if reflectivity has a non-linear dependence on wavelength. The final triplet residues for wavelengths used in the retrieval will be zero.

The first check is of all the non-zero residues; if any is greater than 12.5 in units of N-value, the error flag is set to 5. This condition usually arises when problems in the data stream lead to incorrect values for the measured radiance or when the atmospheric conditions are so unusual that the assumptions used in the calculation of radiances do not hold.

Data that pass flag 5 are checked for sulfur dioxide contamination. The SO_2 index (SOI) is defined by the following equation:

$$r = SOI\left[\frac{dN}{d(SO_2)}\right] + \Delta\Omega\left(\frac{dN}{d\Omega}\right) + b(\lambda - 380) \tag{29}$$

This equation is formulated in the same way as Equation 18, the basic equation for the ozone correction, with an additional term for sulfur dioxide contamination. The physical interpretation is that the mismatch between calculated and measured radiance has a component due to SO_2 in addition to the components due to ozone error, wavelength-dependent reflectivity, and residual calibration error accounted for in Equation 20. Using three wavelengths provides three equations, which can be solved for SOI as a function of the residues, the sensitivities, and the wavelengths. The algorithm uses the residues at 317 nm, 331 nm, and 340 nm. The 312-nm wavelength is not used because it is more affected by aerosols. If the SOI is greater than 24, the error flag is set to 4. The limit corresponds approximately to a 4σ departure from zero, as determined from examination of a day of data that is known not to be contaminated. Since the triplet residues at the wavelengths used to derive the SOI are all zero when the C-triplet is used to derive ozone with the B-triplet to select the profile, SOI is not evaluated for path lengths greater than 3; the output data set will contain a fill value. SO_2-contaminated data will still be likely to be flagged by the remaining residue tests, but the presence of SO_2 will not be identified.

In principle, Equation 29 could be used to simultaneously solve for ozone and SOI. However, the wavelengths best for ozone determination at a given path length are not necessarily the best for SOI determination. Also, the more complicated expression for ozone that would result would significantly increase the computer time required.

The next check assesses triplet consistency. If a single triplet is used, the triplet residue defined in Equation 27 is checked for the ozone-sensitive wavelength not used in the ozone determination: 317 nm in the case of the A-triplet, and 312 nm for the B-triplet. The maximum residues allowed, in N-value units, are 1.1 at 317 nm when an A-triplet determination is checked and 0.9 at 312 nm when a B-triplet determination is checked. If a second triplet is used to determine the profile, then the requirement is that a value of f_{prof} can be found such that $-0.5 \le f_{prof} \le 1.5$. Values of f_{prof} outside this limit require such a degree of extrapolation that the profile is not considered highly reliable. If the data fail the relevant test, the error flag is set to 3. The next check uses the 331-nm residue. If this residue exceeds 4 in N-value units, the error flag is set to 2. Flag values of 3 or 2 resulting from large residues imply that the values of I/F are inconsistent with the assumption that the linear correction can be used.

For solar zenith angles greater than 84 degrees, the algorithm loses accuracy. Most retrievals must make use of the C-pair, which is not highly sensitive to ozone. In addition, the conditions depart from those for which the radiative transfer code was designed, in particular the geometry. For this case, the error flag is set to 1. Finally, because of the summer high zenith angle B/C pair bias discussed in Section 6.6, the value 10 is added to the flag value for the data that are taken in polar summer on the descending (north to south) part of the orbit. While all flagged ozone values appear on the Level–2 data sets, only ozone values with the flag set to 0 for a good retrieval from the ascending part of the orbit are used to derive the gridded means of Level–3.

Table 4.4 summarizes the error flags, when they are set, and their significance.

.

Table 4.4. Error Flags

Flag	Criterion	Significance
0	No other flag set	Good value
1	Solar zenith angle > 84˚	Algorithm less accurate
2	r(331) > 4 (N-value)	Linear correction inadequate
3	r_{trip}(317) > 1.1 (N-value) (if A-triplet alone used) r_{trip}(312) > 0.9 (N-value) (if B-triplet alone used) f_{prof} < -0.5 or f_{prof} > 1.5 (profile selection)	Linear correction inadequate
4	SOI > 24	Sulfur dioxide contamination
5	any residue > 12.5	Unusual atmospheric conditions or data stream problems
+10	Descending orbit	Data taken during descending (north to south) portion of orbit.

5.0 GENERAL UNCERTAINTIES

There are three areas in which uncertainties can be introduced into the ozone derived from TOMS: the accuracy and precision of the measurements, the value of the radiances calculated from the radiative transfer model, and the process of comparing the measured and calculated radiances to derive ozone. In each of these areas, errors of three kinds are possible: random errors, time-invariant systematic errors, and time-dependent systematic errors.

Table 5.1 summarizes the estimated uncertainties in the retrieved Meteor–3 TOMS ozone. They are organized by kind of error rather than by where they originate in the ozone retrieval process. This organization makes it clearer how the errors are to be combined to derive a total error for the retrieval. However, the following discussion will be organized by where the error arises in the retrieval process, to clarify the relationship between the individual uncertainties and how they arise.

Table 5.1. Errors in Retrieved Meteor–3 TOMS Ozone

Source	Error (%)
Random—not applicable to long-term change	
(typical values—may be larger in winter months	
or under disturbed atmospheric conditions)	
Instrument noise (including digitization)	0.3
Atmospheric temperature	1
Retrieval error	2[1]
Tropospheric ozone	1.5
Net (Root sum of squares)	3.0
Time Invariant	
Rayleigh scattering	< 0.5
Ozone absorption cross-section	< 2[2]
Wavelength calibration	< 1
Radiometric calibration	1
Retrieval error	< 1
Net (Root sum of squares)	2.5
Time Dependent	
Radiometric calibration	< 0.5/3yr
Wavelength calibration	< 1.0/3yr
Atmospheric temperature	0.16/°K
Tropospheric ozone	0.05/percent change

[1] May be 5 percent or higher at very high solar zenith angles.
[2] Value for comparisons with non-UV instruments or UV measurements evaluated using different ozone absorption cross-sections.

It is important to recognize that the use of a single number to describe the uncertainty from any source is an oversimplification. In all cases, the uncertainty in total ozone depends upon the wavelengths used in determining ozone, the uncertainty in the measurement at those wavelengths, and the sensitivity of the retrieved ozone to a change in the value of I/F at that wavelength. In addition, the error from a particular source will depend on the conditions of measurement, with values higher than the usual values under certain conditions. The entries in Table 5.1 represent values for the most common conditions. Some cases where the uncertainty may differ significantly from the values in the table are noted.

5.1 Accuracy and Precision of TOMS Measurements

There are three separate components to determining the accuracy and precision of the normalized radiances that are used in the total ozone retrieval from TOMS. First is the precision of the radiances, which is governed by instrument noise and by the digitization of the TOMS output. These factors produce random errors in the value that is given for measured radiance. The second is the initial laboratory calibration. An error in the absolute radiometric calibration or in the wavelength calibration may lead to a time invariant, systematic zero-point error or bias in the retrieved ozone. The third is possible changes with time in the instrument sensitivity. An error here may cause a drift with time of the derived total ozone values.

The largest contributor to random instrumental error, resulting from reporting of raw radiances only at discrete values from the digitized instrument, is less than 0.2 percent at all wavelengths. The total random instrumental error is 0.3 percent. This error is the first entry under random errors in Table 5.1.

Since the initial calibration of V7 Meteor–3 TOMS was adjusted to agree with the Nimbus–7 TOMS, the uncertainty of the initial radiometric calibration is that of Nimbus–7 TOMS, or about 1 percent in derived total ozone. Uncertainties in the radiometric calibration at individual wavelengths may be somewhat larger than this, but since the ozone is derived using wavelength triplets, the impact on derived ozone remains small.

Errors in the instrument wavelength scale also can generate uncertainties in the retrieved ozone. The radiances that are calculated for comparison with measurements must be derived for the wavelengths and slit sensitivity of the TOMS instrument. If there is an error in the wavelengths assumed, then the calculated radiances will not be the same as those actually measured by the TOMS instrument, leading to an error in the retrieved ozone. As discussed in Section 3.3, it is estimated that the initial TOMS wavelength calibration was known to ±0.1-nm accuracy. This uncertainty corresponds to a possible systematic error of less than 1 percent in derived ozone, constant with time.

A wavelength calibration drift could produce a time-dependent error in ozone. As noted in Section 3.3, the wavelength calibration drifted by less than 0.04 nm over the life of the instrument, corresponding to a possible drift of less than 1.0 percent in ozone over the instrument lifetime. The upper limit to the possible change appears on the first line under the time-dependent changes of Table 5.1.

The uncertainty in the time dependence of the radiometric calibration is estimated to be less than 0.5 percent in ozone over the instrument lifetime. This uncertainty is small relative to the Nimbus–7 TOMS because of the diffuser carousel used for Meteor–3. This situation is illustrated in Figure 3.1 by the fit of the 313-nm to 360-nm ratio. It is the uncertainty in the determination of the wavelength dependent calibration that is critical to the TOMS total ozone determination.

5.2 Calculated Radiances and Their Use in the Algorithm

Errors in the calculation of radiances have two principal origins: in the physical quantities whose values are obtained from laboratory physics and in the atmospheric properties assumed for the radiative transfer calculations. Calculation of the scattering of atmospheric radiation by ozone and the other constituents of the atmosphere requires values for the ozone absorption and Rayleigh scattering coefficients. The values used in the algorithm are obtained from laboratory measurements. Any error in the laboratory values will propagate through the algorithm to produce a systematic error in the derived ozone. The first two lines in the time-invariant error group of Table 5.1 show the effect of the uncertainties in these quantities on derived ozone. In addition, the absorptivity of ozone is a function of the temperature. The calculated radiances are based upon a climatological temperature (Appendix A) however, if the temperature structure departs from the climatology, the absorption coefficient may change from that assumed in the algorithm, producing an error in retrieved ozone. The size of this error is shown in the second line of the random error group.

The third random error component listed in Table 5.1, called retrieval error, arises from variations of the properties of the real atmosphere about those assumed for the calculation of radiances. The most important of these is the difference between the actual vertical distribution of ozone and the standard profile used to compute the look-up tables. At low to moderate solar zenith angles, the TOMS derived total ozone is not significantly dependent on the ozone profile used. At high solar zenith angles, however, profile sensitivity is a significant source of error. The profile interpolation procedure described in Section 4.5 reduces this error, but does not eliminate it. Because of its precessing orbit, more of the Meteor–3 data relative to Nimbus–7 were taken at high solar zenith angles. Because of this and the impact of high solar zenith angles on the TOMS retrieval, we have increased the algorithmic contribution to random errors for Meteor–3 relative to Nimbus–7 TOMS from 1 percent to 2 percent.

The fourth random error in Table 5.1 arises from possible variations in tropospheric ozone, in particular from cases where changes in tropospheric ozone do not affect the measured radiance. TOMS cannot measure ozone that is hidden from the instrument by thick cloud. In the TOMS algorithm, a climatological tropospheric ozone amount is

assumed to be present beneath the cloud fraction identified by the reflectivity channel of TOMS. Thus, the error due to hiding by clouds in a given measurement is equal to the error in tropospheric ozone times the cloud fraction, and the algorithm will, in general, be less sensitive to errors in tropospheric ozone if the cloud fraction is low. About 6 percent of total ozone is in the lowest 5 km, with a 50 percent variability. The radiation from the troposphere has both surface and atmospheric components: the surface component traverses the troposphere and provides a measure of tropospheric ozone, while the atmospheric component, arising from Rayleigh scattering, is not as sensitive to the ozone amount. Over surfaces with low reflectivity, the Rayleigh scattering component dominates, and the measured radiance will not be sensitive to departures from the standard tropospheric ozone profile. When the surface is highly reflective, the ozone-sensitive surface component is more important, and the TOMS estimate of tropospheric ozone improves; thus, the problem of tropospheric ozone is less significant over ice-covered regions such as the Antarctic. The retrieval also improves at low solar zenith angles when incident UV penetrates further into the troposphere (Klenk et al. 1982). Overall, TOMS measures roughly half of the trophospheric ozone variation.

Assignment of the temperature, retrieval, and tropospheric ozone errors as random is based upon an approach in which the atmospheric variations are not known and are treated as random variability about the climatology. However, if independent measurements of any of these quantities are available for a scan, then such measurements can be used to correct the ozone values derived from TOMS, and the error would no longer be random. The next section discusses such corrections.

5.3 Estimating Sensitivities to Atmospheric Conditions

Independent measurements of tropospheric ozone or atmospheric temperature make it possible to evaluate the contribution of these changes to the derived ozone. This contribution may then be treated as a systematic, time-dependent contribution, whose size is given by the sensitivity of the derived ozone to the known variations in these quantities, rather than as a random error. The last two entries under time-dependent error show the sensitivities that can be used to determine the corrections to ozone that should be applied for known changes in atmospheric temperature and tropospheric ozone.

5.4 Comparison with Nimbus TOMS

Meteor–3 TOMS has a 1.5-year overlap with the Nimbus–7 TOMS instrument. As discussed in Section 3.2, the initial calibration of Meteor–3 TOMS has been adjusted to agree with Nimbus–7 TOMS, but the time-dependent calibrations of the two instruments are independent. Figure 5.1 shows the difference of daily zonal means of total ozone amount computed using the Level–3 products from the two instruments. The shaded areas indicate portions of the Meteor–3 TOMS Level–3 product that are not included in the archive, as discussed in Section 2.4. These are periods when the Local Equator Crossing Time (LECT) of the sunlit portion of the Meteor–3 orbit is before 9:00 a.m. or after 3:00 p.m. during the first data year and before 8:00 a.m. or after 4:00 p.m. during the remainder of the instrument lifetime (Table 2.1). The tighter limitations in the first data year are applied because of the strong impact of aerosols from Mt. Pinatubo during this period. During the shaded periods, the Meteor–3 TOMS is making measurements in extreme geometries that degrade the accuracy of the retrieval, particularly in the presence of volcanic aerosols which are not modelled in the radiative transfer calculations of theoretical radiances in the TOMS retrieval. It is clear in the figure that some residual angular dependence exists in the archive data. It is generally less than 2–3 percent. There is a small residual bias between the two instruments of slightly less than 1 percent which is within the uncertainties of the technique used to normalize the two instruments. There may be a slight downward trend in the bias which is probably due to growing uncertainty in the Nimbus–7 TOMS time-dependent calibration near the end of its lifetime (Wellemeyer et al., 1996). All of the Meteor–3 TOMS data are available in Level–2 format, but users are cautioned regarding the use of data taken at the extreme geometries associated with near terminator orbits of the Meteor–3.

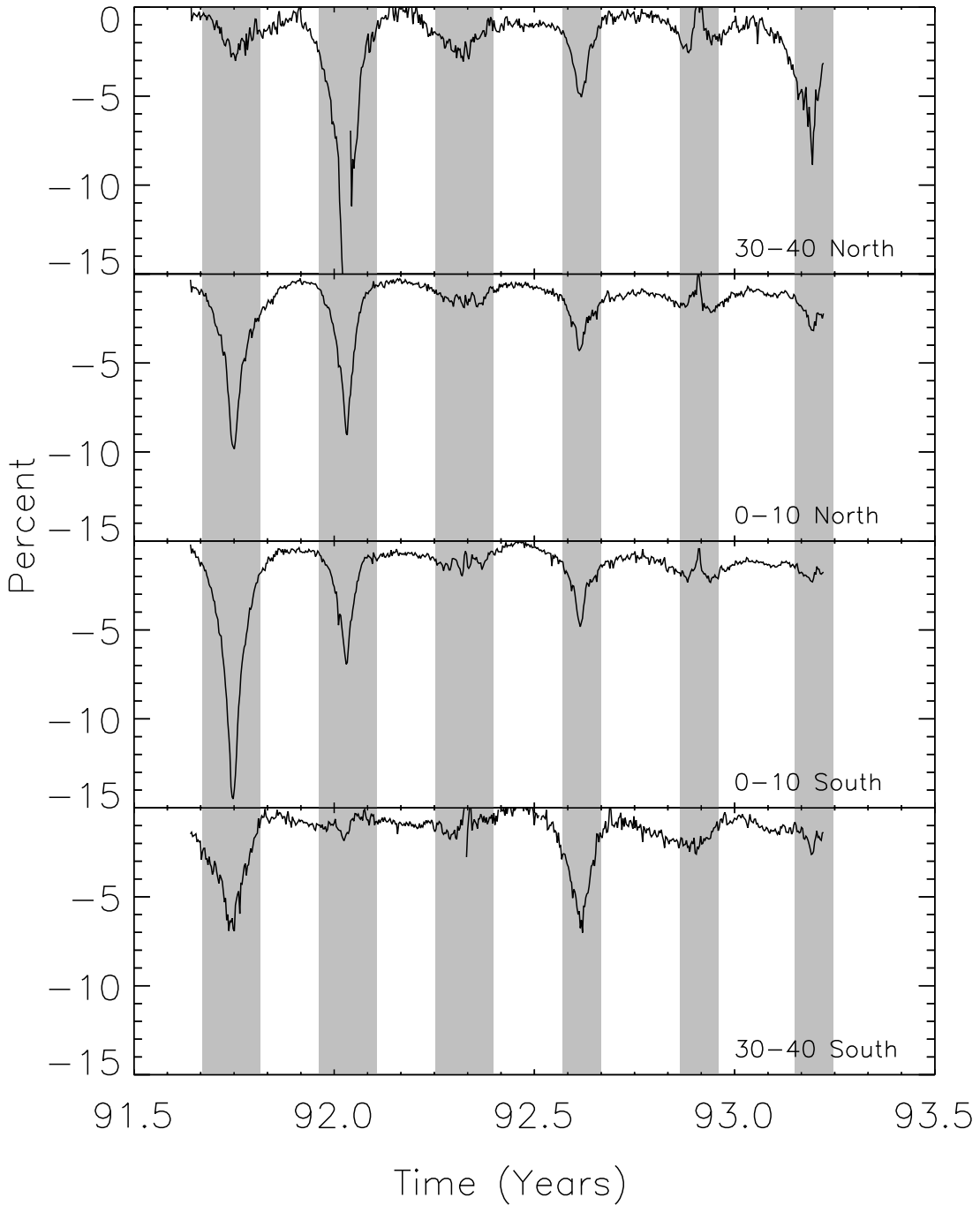

Figure 5.1. Meteor–3 Nimbus–7 TOMS Ozone Comparison

5.5 COMPARISON WITH GROUND-BASED MEASUREMENTS

The Meteor–3 TOMS Version 7 data have been compared with ground based measurements made by a network composed of 30 mid-northern latitude stations with Dobson and Brewer ozone measuring instruments. This is the same set of stations used in comparisons of Nimbus–7 TOMS with ground-based measurements [McPeters et al., 1996]. Each ground measurement was paired with the TOMS sample whose center was closest to the station; if two measurements were equally near, the one measured closest to nadir was used. A weekly mean was then calculated of the daily TOMS-ground differences at each station. These means were then averaged to derive a weekly average TOMS-network difference.

Figure 5.2 shows the percentage difference of TOMS - ground ozone measurements as a function of time. Only those periods of time for which the Level–3 data are archived are shown in the figure. Although the bias tends to be larger at the higher solar zenith angles near the periods of missing data, it is still smaller than the combined uncertainty of the two measurement systems and the comparison technique. There is no significant trend in the bias, so only the mean bias and its standard deviation are noted in the figure.

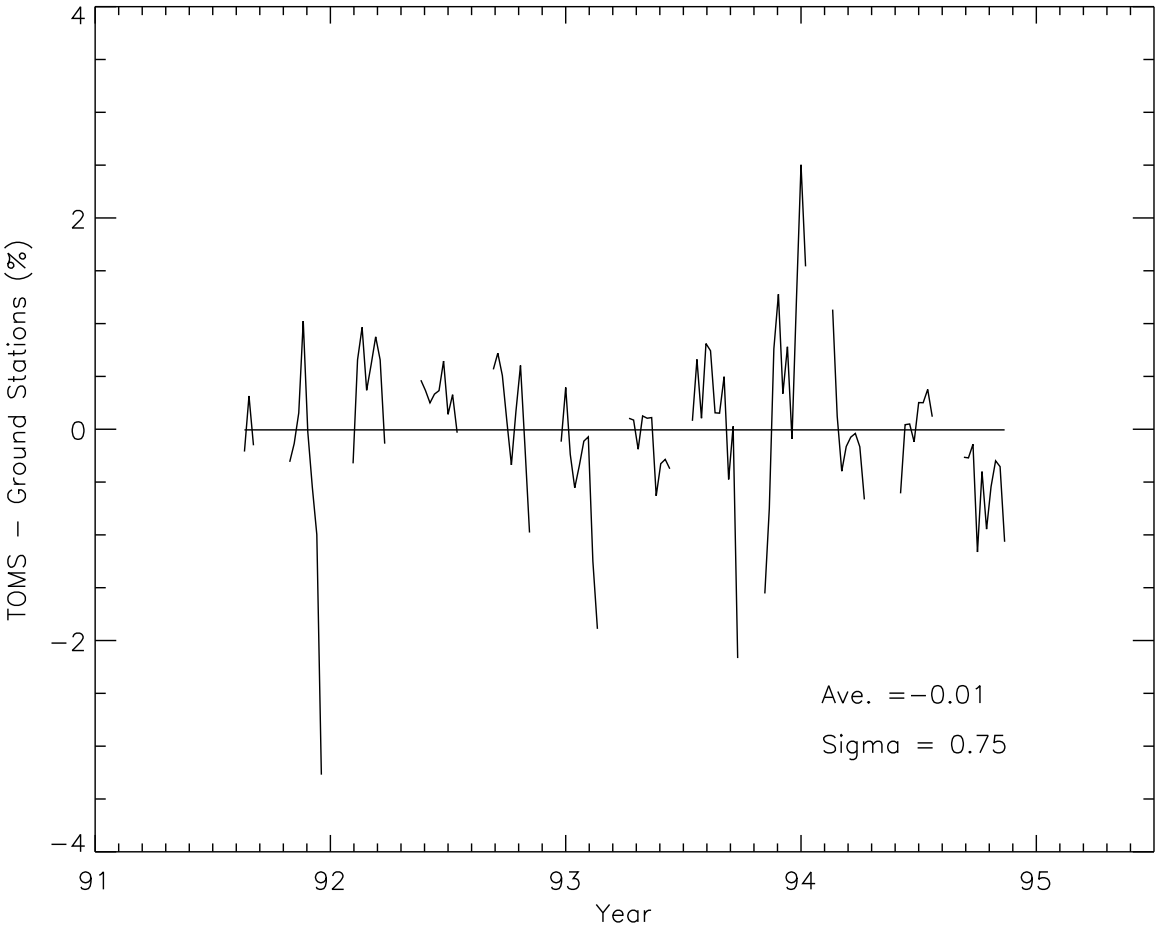

Figure 5.2. Percentage Difference Between TOMS and Ground-Based Measurements of Ozone. Solid line is the mean bias.

6.0 PROBLEMS LOCALIZED IN SPACE AND TIME

6.1 Volcanic and Aerosol Contamination

Increased Mie scattering by sulfuric acid aerosols in the atmosphere modifies its radiative transfer properties and may significantly affect the backscattered ultraviolet radiances measured by TOMS. Depending on the solar and satellite zenith angles, the effect may be either an enhancement or a reduction in the measured radiances. The magnitude of the effect depends upon the optical depth of the aerosol layer and its altitude with respect to the ozone peak, being greatest for those wavelengths whose contribution function peaks in the vicinity of the densest part of the ozone layer (Torres and Bhartia, 1995). The SBUV spectral scans of Earth radiance show this effect to be most significant at wavelengths shorter than those used by TOMS for the retrieval of total ozone. During the first two years after launch, the ozone retrieved by the Meteor–3 TOMS instrument was affected by the scattering effects of the stratospheric sulfate aerosol layer formed in the aftermath of the eruption of Mt. Pinatubo in The Philippines on June 15, 1991. As discussed by Bhartia, et al. (1993) and Torres, et al. (1995), the optically thick sulfate aerosol layer introduces a strong angular dependence that can be easily observed in the zonally averaged ozone data plotted as a function of scan angle, or the more physically relevant scattering angle. Figure 6.1 shows the evolution of the TOMS scan angle bias from 1991 to 1994 at 10°N for similar viewing conditions (in terms of scattering angle). The retrieved ozone is generally overestimated for scattering angles between 100 and 155 degrees and underestimated for scattering angles less than 100 degrees and larger than 155 degrees. At scattering angles between 95 and 100 degrees and between 150 to 155 degrees the aerosol induced error is minimum.

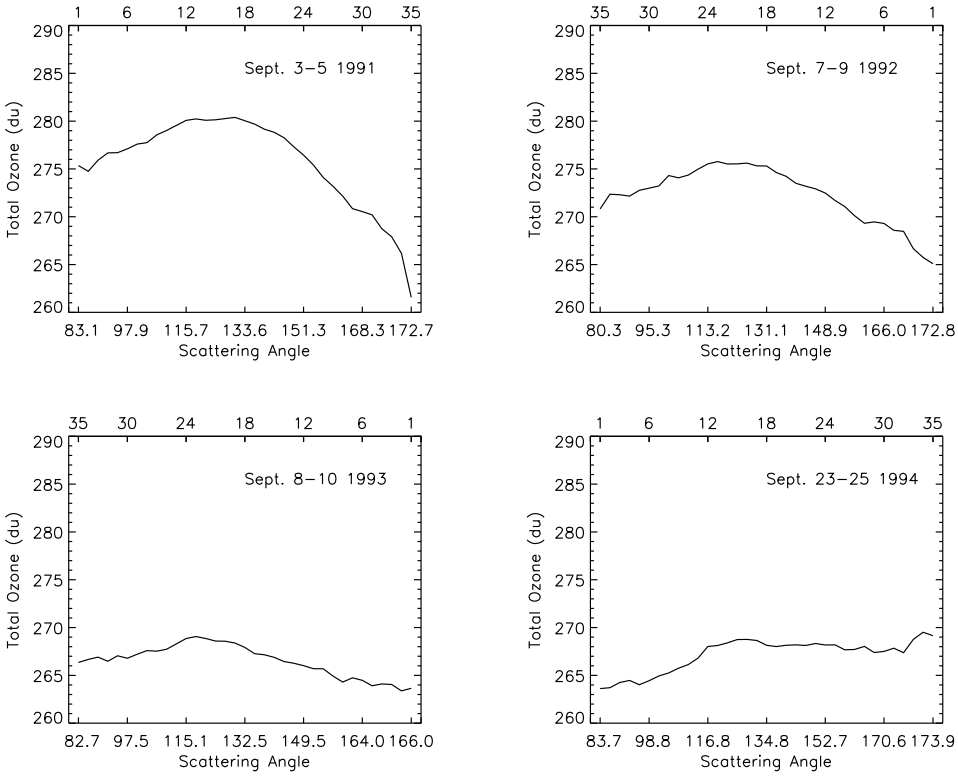

Figure 6.1 Scan Angle and Scattering Angle Dependence of Meteor–3 TOMS Ozone. Evolution of Meteor–3 TOMS average scan angle dependence induced by the waning Pinatubo aerosols over the course of the experiment. TOMS retrieval is least affected at scattering angles of 155 degrees. The upper left and right panels are from ascending (south to north) orbits in the morning and afternoon, respectively. The lower left and right panels are from descending orbits in the afternoon and morning respectively. Data in the upper left panel are not included in the Level–3 archive (see Table 2.1). TOMS scan position is indicated on the upper horizontal axis (18-nadir, 1-extreme right, 35-extreme left).

6.2 Additional Scan Angle Dependence

For near local noon equator crossing times, Sun glint can occur over water for clear sky and near overhead Sun. Under these conditions, the derived surface reflectivity is enhanced, a result of scattering by the stratospheric background of the extra radiation reflected from the surface. The consequence is that derived ozone is about 1 percent low under these conditions near nadir in the vicinity of the center sample.

6.3 Solar Eclipses

When the Sun is eclipsed, the decrease in incoming solar irradiance leads to a decrease in the backscattered Earth radiance. However, because the solar irradiance used for the ozone retrieval is derived from measurements of the uneclipsed Sun, the derived I/F is not correct during times of eclipse. Consequently, ozone values are not retrieved for periods of time and ranges of latitude where the radiances are affected by a solar eclipse. In actual production, tabulated eclipse information is part of the input stream for the job run and is used by the software to exclude the eclipse periods and regions.

6.4 Polar Stratospheric Clouds

The effect of anomalously high clouds can be a significant error source for localized regions in the Arctic and Antarctic. Polar Stratospheric Clouds (PSCs) above the ozone peak may cause the TOMS retrieved total ozone to be underestimated for solar zenith angles larger than 70 degrees. Models indicate that the impact of these clouds on TOMS retrieved total ozone is a strong function of optical depth. Type I PSCs of optical depth 0.01 (composed of $HNO_3/3H_2O$, particle mean radius ~0.5 μm) may produce an underestimate of up to 2 percent at solar zenith angles greater than 80 degrees. Larger errors (up to 6 percent) may be introduced by Type II PSCs of optical depth 0.05 (water ice, particle mean radius ~5–50 μm). Underestimates as large as 50 percent may occur when Type II PSCs of optical depth 0.4 (associated with lee-waves) are present. No corrections have been made for the presence of PSCs, but they tend to be very localized in time and space, lasting 3–5 days with typical sizes of 1000–3000 km (Torres et al., 1992).

6.5 High Terrain

Users may note an apparent anticorrelation of ozone with terrain height, particularly in the form of ozone dips above high mountain ranges. These dips occur because the algorithm retrieves the actual column ozone above the surface, not above sea level. The atmospheric ozone that would normally be present between sea level and the actual terrain height is missing. Column ozone actually is lower above the mountains, in the same way as other atmospheric constituents. The relation between column ozone and altitude is thus not an artifact of the measurement but simply reflects the fact that when the surface is higher, there is less atmosphere above it.

6.6 Measurements at High Solar Zenith Angle over the Summer Pole

For a period around the summer solstice for each pole, TOMS is able to measure backscattered sunlight from the polar regions on the ascending (south to north) as well as the descending (north to south) part of the orbit. The ozone values derived at the higher solar zenith angles are biased low. As zenith angle increases, so does the path length, and the algorithm switches from the B-triplet to the C-triplet. The C-triplet has proven to have a seasonally dependent bias relative to the B-triplet, with the C-triplet approximately 4 percent lower in summer and with the bias approximately zero in winter. Thus, the low values for high zenith angle reflect the shift to the C-triplet and its biasing low. The origin of this bias is not currently understood. Fortunately, this problem does not strongly affect the TOMS coverage or the Level–3 map product. In summer, the biased measurements are redundant as they are available from the other portion of the orbit. In winter, when the high zenith angle data must be used, the bias is small. When the Level–3 product is created, the redundant high solar zenith angle retrievals are not used. As the Meteor–3 orbit precesses close to the terminator, both ascending and descending portions of the orbit may be using C-triplet. These data are also excluded from the Level–3 archive as discussed in Section 2.4. However, users of the Level–2 product should be aware of this problem and avoid the use of these data.

7.0 DATA FORMATS

7.1 Hierarchical Data Format

TOMS data products will be available electronically from the Distributed Active Archive Center (DAAC) in the form of Hierarchical Data Format (HDF) files (Ilg et al., 1993; Kalman, 1994). Along with the files, the DAAC will distribute HDF software tools for reading the files.

7.1.1 Level–2 Hierarchical Data Format Product

The standard archival Level–2 products are stored in HDF files, one for each orbit, at the GSFC DAAC. They are generated using the most recent version of HDF available from the University of Illinois' National Center for Supercomputing Applications (NCSA) and endorsed by the Earth Observing System Data Information System (EOSDIS) Project. The Level–2 file contains all output from the Version 7 ozone processing, including ozone and reflectivity products, as well as diagnostic parameters and a SOI, on a scan-by-scan basis for each TOMS daylit FOV.

The Level–2 HDF file consists of the following components:

1. A File Label
2. A File Description
3. Metadata (stored as a second file description)
4. Network Common Data Form (netCDF) style attributes
5. Multiple Data Scientific Data Sets (SDSs)
6. Multiple Coordinate SDSs

The File Label is a string that identifies the instrument, the spacecraft, date, and orbit number of the data within the Level–2 HDF. It has the following form: “TOMS_METEOR–3_yyddd.nxxxxx”, where yy is the (two digit) year, ddd is the three-digit day of year, and xxxxx is the lifetime orbit number (i.e., revolution since launch, where orbit 1 is defined to start with the first ascending node equator crossing). Leading zeroes are used for yy, ddd, and xxxxx when applicable.

The File Description is a field of up to 40,000 ASCII characters which describes, in free form text, the Level–2 product and its generation algorithm.

Metadata include the following:

1. Data set name
2. Data product name
3. Granule size (bytes)
4. Time of first scan of orbit (year, month, day, hour, minute, second, GMT)
5. Time of last scan of orbit (year, month, day, hour, minute, second, GMT)
6. Number of scans (including fill) in orbit
7. Date and time of ascending node equator crossing (year, month, day, hour, minute, second, GMT)
8. Longitude of ascending node equator crossing (degrees; –7777 when unavailable)
9. Altitude of spacecraft during last TOMS scan of orbit (km)
10. Orbit number
11. Geographical flag - o (orbit) for Level–2
12. Day/night flag
13. Granule version
14. Producer granule ID
15. 4 byte signed decimal integer that represents missing value
16. 2 byte signed decimal integer that represents missing value
17. 1 byte unsigned decimal integer that represents missing value

The following netCDF style attributes are included:

1. Quality flag counters (32)
   1 Number of input/output errors for this orbit
   2 Number of scans read for orbit
   3 Number of scans written for orbit
   4 Number of samples out of range (total)
   Number of samples out of range for
   5 Zenith angle > 88 degrees
   6 Latitude
   7 Instrument counts (negative)
   8 Number of samples written that were bad (total)
   Numbers of individual error flags for Algorithm Flag = 1 (see Table 7.2 for description of error and algorithm flags):
   9 Number of samples that had error flag = 0 or 10
   10 Number of samples that had error flag = 1 or 11
   11 Number of samples that had error flag = 2 or 12
   12 Number of samples that had error flag = 3 or 13
   13 Number of samples that had error flag = 4 or 14
   14 Number of samples that had error flag = 5 or 15
   15–20 Same as 9–14 for Algorithm Flag = 2
   21–26 Same as 9–14 for Algorithm Flag = 3
   27–32 Same as 9–14 for Algorithm Flag = 4
2. TOMS band center wavelengths (nm), shortest first
3. Solar irradiance F-values at 1 A. U. (watts/cm^3) for the current day at the six TOMS wavelengths, shortest first
4. Count-to-radiance conversion factors (watts/cm^3/steradian/count) for each of the four gain ranges for each of the six wavelengths, shortest first
5. Nominal spacecraft zenith angle (degrees) at each scan position

There are 27 Data SDSs stored in the Level–2 product. Their names, dimensions and data types are listed in Table 7.1. More detailed descriptions, units, offsets, and scale factors are listed in Table 7.2. The data are stored as integers; to convert to the physical units, they must be added to the offset and then multiplied by the scale factor. Table 7.3 lists the fill values used for different data types for missing scans. One-dimensional SDSs are stored in a TOMS scan number domain. Two-dimensional SDSs are stored in a TOMS scan number by TOMS scene number domain. Three-dimensional SDSs are stored in a TOMS scan number by TOMS scene number by TOMS wavelength domain.

The four Coordinate SDSs stored in the Level–2 product are listed in Table 7.4.

Table 7.1. TOMS Level–2 HDF SDSs

Name of SDS	Dimensions	Data Type
LSEQNO	575	2 byte integer
YEAR	575	2 byte integer
DAY	575	2 byte integer
GMT	575	4 byte integer
ALTITUDE	575	2 byte integer
NADIR	575	2 byte integer
SYNC	575	2 byte integer
LATITUDE	575 x 35	2 byte integer
LONGITUDE	575 x 35	2 byte integer
SOLAR_ZENITH_ANGLE	575 x 35	2 byte integer

Table 7.1. TOMS Level–2 HDF SDSs (Continued)

PHI	575 x 35	2 byte integer
NVALUE	575 x 35 x 6	2 byte integer
SENSITIVITY	575 x 35 x 5	2 byte integer
dN/dR	575 x 35 x 6	1 byte unsigned integer
RESIDUE	575 x 35 x 5	1 byte unsigned integer
TOTAL_OZONE	575 x 35	2 byte integer
REFLECTIVITY	575 x 35	2 byte integer
ERROR_FLAG	575 x 35	2 byte integer
OZONE_BELOW_CLOUD	575 x 35	1 byte unsigned integer
TERRAIN_PRESSURE	575 x 35	1 byte unsigned integer
CLOUD_PRESSURE	575 x 35	1 byte unsigned integer
SOI	575 x 35	1 byte unsigned integer
ALGORITHM_FLAG	575 x 35	1 byte unsigned integer
CLOUD_FRACTION	575 x 35	1 byte unsigned integer
MIXING_FRACTION	575 x 35	1 byte unsigned integer
CATEGORY	575 x 35	1 byte unsigned integer
THIR_CLOUD_PRESSURE	575 x 35	1 byte unsigned integer

The last index varies most rapidly in all arrays.

Table 7.2. Detailed Description of TOMS Level–2 SDSs

SDS Name	Description
LSEQNO	Sequence number of scan within orbit
YEAR	Year (four digits) at start of scan, GMT.
DAY	Day of year (1–366) at start of scan, GMT.
GMT	Greenwich Mean Time in seconds of day at start of scan (1–86,400).
ALTITUDE	Spacecraft altitude at start of scan (km).
NADIR	Nadir scan angle, used to express the spacecraft's attitude error, the angle between the vectors from the S/C to the local normal and from the S/C to the FOV ($0 \leq$ nadir angle ≤ 180) (x 100).
SYNC	Flag for chopper non-synchronization occurrence: 0: Does not occur in current or next scan 1: Occurs in current scan, not in next 2: Occurs in next scan, not current 3: Occurs in both current and next scan
LATITUDE	IFOV latitude, from 90˚ S–90˚ N (degrees x 100).
LONGITUDE	IFOV longitude, from 180˚ W–180˚ E (degrees x 100).
SOLAR_ZENITH_ANGLE	IFOV solar zenith angle (degrees x 100).
PHI	Angle ϕ between sun and satellite measured at IFOV, (degrees x 100).
NVALUE	N-values (as defined in Section 4.5) at 6 wavelengths, shortest first (x 50).
SENSITIVITY	Sensitivity dN/dΩ at 5 shortest wavelengths, shortest first, obtained by table interpolation (matm-cm^{-1} x 10,000).
dN/dR	N-value sensitivity to reflectivity dN/dR at 6 wavelengths, shortest first (%$^{-1}$ x –50).
RESIDUE	Adjusted residues (see Sections 4.5) at 5 shortest wavelengths, shortest first (x 10 + 127).
TOTAL_OZONE	Total Ozone (matm-cm), x 10.
REFLECTIVITY	Effective reflectivity assuming Lambertian surface (% x 100).

Table 7.2. Detailed Description of TOMS Level–2 SDSs (Continued)

SDS Name	Description
ERROR_FLAG	Error Flag 0 good data 1 good data, 84˚ < solar zenith angle < 88˚ 2 residue at 331 nm greater than 4 in N-value units 3 triplet residue too large (A-triplet: r_{317} > 1.1 N-value units) (B-triplet: r_{312} > 0.9 N-value units) (f_{prof}: < –0.5 or > 3.5) 4 SOI > 24 (SO_2 contamination) 5 At least one residue has absolute value larger than 12.5 A value of 10 is added to the error flag for all scans on descending (midnight) part of orbit.
OZONE_BELOW_CLOUD	Estimated ozone below cloud layer (matm-cm).
TERRAIN_PRESSURE	Ground pressure derived from NOAA/NMC grid (atm x 100).
CLOUD_PRESSURE	Cloud pressure from ISCCP climatology (atm x 100).
SOI	Sulphur dioxide index (SOI), (matm-cm + 50).
ALGORITHM_FLAG	Algorithm flag - identifies triplet(s) used 1: A-triplet alone used 2: B-triplet alone used 3: B-triplet with A-triplet to select profile 4: C-triplet with B-triplet to select profile
CLOUD_FRACTION	Effective cloud fraction, as defined in Section 4.3 (percent).
MIXING_FRACTION	Mixing fraction f_{prof}, which parameterizes contributions of lower and higher latitude profiles in ozone determination, as described in Section 4.5; values range from 0.5 to 3.5 (x 10). 1: pure low latitude 2: pure mid latitude 3: pure high latitude
CATEGORY	Surface Category code 0: ocean 1: land 2: low inland (below sea level) 3: mixed land and ocean 4: mixed land and low inland 5: mixed ocean, land, and low inland
THIR_CLOUD_PRESSURE	Cloud pressure measured from Temperature-Humidity Infrared Radiometer, where available, (atm).

Table 7.3. Fill Values for Missing Scans

Data Type	Decimal	Hexadecimal
1 byte unsigned integer:	255	xFF
2 byte integers:	32767	x7FFF
4 byte integers:	2147483647	x7FFFFFFF

Table 7.4. TOMS Level–2 HDF Coordinate SDSs

Name	Type	Scaletype	Scalemin	Scalemax
time_of_orbit	2 byte int	regular	0	#scans-1
scan_position	2 byte int	regular	0	#scans-1
wavelength_6	4 byte real	irregular	n/a (6 TOMS wavelengths)	
wavelength_5	4 byte real	irregular	n/a (5 shortest wavelengths)	

7.1.2 Level–3 Hierarchical Data Format Product

The standard archival Level–3 product contains global arrays of total ozone and effective surface reflectivity stored as daily HDF files. A Level–3 file is generated from each complete daily set of Level–2 files.

The Level–3 HDF file is comprised of the following elements:

1. a File Label,
2. a File Description,
3. Metadata (stored as a second file description),
4. 2 Data Scientific Data Sets (SDS),
5. 2 Coordinate SDSs.

The Level–3 file names have the following form:

m3gYYDDD.hdf
where YY is a 2-digit year and DDD is day of year.

The File Description provides background on the TOMS instrument, processing algorithms and data products, in free format. The following metadata are included:

1. Data set name
2. Data product name
3. Granule size (bytes)
4. Begin date and time (year, month, day, hour, minute, second, GMT)
5. End date and time (year, month, day, hour, minute, second, GMT)
6. Geographical flag - G (grid) for Level–3
7. Locations (latitude and longitude) of 4 corner points
8. Day/night flag
9. Granule version
10. Producer granule ID
11. Value representing missing data for ozone
12. Value representing missing data for reflectivity
13. Equator crossing time of first orbit (year, month, day, hour, minute, second, local mean solar time)

The data stored in the SDSs are on a fixed 1-degree latitude by 1.25-degree longitude grid. The gridded ozone values are stored as 3-digit integers in units of matm-cm. Reflectivity in percent, is also stored as 2-byte integers. Grid cells that are missing data due to lack of sunlight or other problems will be filled with 0 for ozone, 999 for reflectivity.

The two Coordinate SDSs stored in the Level–3 product are listed in Table 7.5.

Table 7.5. TOMS Level–3 HDF Coordinate SDSs

Name	Type	Scaletype	Scalemin	Scalemax
Latitude	4 byte real	regular	–89.5	89.5
Longitude	4 byte real	regular	–179.375	179.375

7.2 Native Format

7.2.1 TOMS Ozone File (Level–2 Data Product)

The TOMS Ozone File, also called the Level–2 Data Product, is a binary file, written as FORTRAN unformatted records. It is generated under UNIX. These files are used primarily as part of the TOMS processing. They are not normally distributed but may be obtained by special arrangement.

Each file contains all of the data processed for a single day. The first record of the file is a header, written in character format, containing information on the production hardware and software for both the Level–2 product and the Level–1 product used to generate it, the date and time the Level–2 file was generated, and the time period that the data on the file cover. The data records follow, ordered chronologically by time (GMT) of observation, and grouped by TOMS orbit. Each data record contains the information processed from one scan of the TOMS instrument. Only daylight scans, where the solar zenith angle at the nadir view for the scan is less than or equal to 92 degrees, have been processed by the ozone algorithm and written to the ozone file. The end of an orbit is indicated by a record called the orbital summary record, which contains the date, time, and location of the start and end of the orbit and of the equator crossing, counts of the number of scans processed and those flagged for various reasons, and other summary and ancillary information for the orbit. The last record of the file, called the trailer record, contains the time and date of the first and last scan of the last orbit of the day and the total number of the scans processed and flagged for various reasons for all orbits.

Each type of record, other than the header, can be identified by the logical sequence number, which is stored as an integer in the two most significant bytes of the third word of the record. All data records have a positive logical sequence number that counts the order of that record within the orbit to which it belongs, starting with a value of 1 for the first data record of the orbit. The orbital summary record for each orbit has a *negative* logical sequence number whose absolute value is one greater than that of the last data record of the orbit. The trailer record contains the unique logical sequence number of –1, which may be used to identify the end of the file.

Tables 7.6–7.10 contain, in order, the format of the header record, the format of the data records, a detailed description of selected words in the data record, the format of the orbital summary record, and the format of the trailer record.

Table 7.6. Format of TOMS Ozone File Header Record

Bytes	Character Representation*	Description
1–9	METEOR–3	Spacecraft identification.
10–14	FM-2_b	Flight model identifier. 1= Nimbus 2= Meteor
15–22	LEVEL–2_b	Data product identification
23–38	$BY_bXXXXXXXXXXX_b$	Program name in 12 characters, e.g., ozt.f
39–51	$VERSION_bXXXX_b$	Program version in 4 characters, e.g., 1.0
52–63	$MMM_bDD_bYYYY_b$	Program date in month-day-year, e.g., JUL 01 1994
64–83	$ON_bXXXXXXXXXXXXXXX_b$	Processing environment, 16 char., e.g., ALPHA UNIX V
84–106	$GEN_bMMM_bDD_bYYYY_bHHMMSS_b$	Time in month, day, year, hours, minutes, and seconds, corresponding to generation time of file.
107–135	$DATA_bSPAN_bMMM_bDD_bYYYY_bHHMMSS_b$	Time in month, day, year, hours, minutes, and seconds, corresponding to start of data span on file.
136–159	$TO_bMMM_bDD_bYYYY_bHHMMSS_{bbb}$	Time in month, day, year, hours, minutes, and seconds, corresponding to end of data span on file.
160–174	LEVEL–$1_bHEADER:_b$	Indicates that actual Level–1 header follows.
175–2100	[Level–1 header]$_{b\cdots b}$	Actual text of Level–1 header, followed by spares.

* Character "$_b$" is used to indicate a blank character.

Table 7.7. Format of Data Records

Word	Byte 1	Byte 2	Byte 3	Byte 4
1	Orbit number			
2	GMT (seconds of day) at start of scan			
3	Logical sequence number		Chopper synchronization flag	
4	Day of year at start of scan		Year at start of scan	
5	Altitude		Sample 1 view angle	
6	Latitude		Longitude	
7	Solar Zenith Angle		ϕ Angle	
8	N_{312}		N_{317}	
9	N_{331}		N_{340}	
10	N_{360}		N_{380}	
11	$(dN/d\Omega)_{312}$		$(dN/d\Omega)_{317}$	
12	$(dN/d\Omega)_{331}$		$(dN/d\Omega)_{340}$	
13	$SENS_{360}$		Reflectivity	
14	Total Ozone		Error Flag	
15	$(dN/dR)_{312}$	$(dN/dR)_{317}$	$(dN/dR)_{331}$	$(dN/dR)_{340}$
16	$(dN/dR)_{360}$	$(dN/dR)_{380}$	THIR cloud pressure	Terrain pressure
17	$RES(N_{331})$	$RES(N_{317})$	$RES(N_{331})$	$RES(N_{340})$
18	$RES(N_{360})$	Ozone Below Cloud	SOI	Cloud pressure
19	Algorithm Flag	Eff. Cloud Fraction	Mixing Fraction	Surface Category
20-523	Same as 6 through 19 for samples 2 to 35			
524-525	Spares			

Notes:
All values are stored in INTEGER format, MSB first. Values stored in one byte are always positive, with a value of 255 indicating missing data. Values stored in two bytes can be either positive or negative, with values of 32767 indicating missing data. Some values have had constants added or multiplied to accommodate integer storage.

Table 7.8. Detailed Descriptions

Word	Bytes	Description
1		Orbit number, starting at ascending node
2		Greenwich Mean Time at start of scan in seconds (1–86,400)
3	1–2	Sequence number of record in file
	3–4	Flag for chopper non-synchronization:
		0 Does not occur in current or next scan
		1 Occurs in current scan, not in next
		2 Occurs in next scan, not current
		3 Occurs in current and next scan
4	1–2	Day of Year (1–366) at start of scan
	3–4	Year at start of scan (4 digits)
5	1–2	Spacecraft altitude in kilometers at start of scan

Table 7.8. Detailed Descriptions (Continued)

Word	Bytes	Description
	3–4	Sample 1 view angle can be used to calculate the nominal spacecraft roll error and the 35 view angles within each scan. The view angle is the angle between the FOV local normal vector and the vector from the FOV to the spacecraft. The relationship between roll angle and the 35 view angles in a scan is given by $$V_n^* = V_n + \frac{r_e + h_s}{r_e}\frac{\cos(S_n)}{\cos(V_n)}\Delta R$$ where V_n^* is the actual view angle for sample number n, V_n is the nominal view angle for sample n (given in the orbital summary trailer record), S_n is the nominal scan angle for sample number n, ΔR is the roll angle, r_e is the radius of the earth (6,380 km), h_s is the height of the satellite (955 km). The scan angle is the angle between the vectors from the S/C to the local normal and from the S/C to the FOV, and ranges in 3-degree steps from 51 degrees at sample 1 to 0 degrees at nadir back to 51 degrees at sample 35.
6	1–2	IFOV latitude, from 90˚ S–90˚ N, in degrees x 100
	3–4	IFOV longitude, from 180˚ W–180˚ E, in degrees x 100
7	1–2	IFOV solar zenith angle, in degrees x 100
	3–4	Angle ϕ between sun and satellite measured at IFOV, in degrees x 100
8	1–2	213 nm N-value x 50 (N-value is defined in Section 4.5)
	3–4	317 nm N-value x 50
9	1–2	331 nm N-value x 50
	3–4	340 nm N-value x 50
10	1–2	360 nm N-value x 50
	3–4	380 nm N-value x 50
11	1–2	312 nm sensitivity dN/dΩ, in $(\text{matm-cm})^{-1}$ x 10,000
	3–4	317 nm sensitivity dN/dΩ, in $(\text{matm-cm})^{-1}$ x 10,000
12	1–2	331 nm sensitivity dN/dΩ, in $(\text{matm-cm})^{-1}$ x 10,000
	3–4	340 nm sensitivity dN/dΩ, in $(\text{matm-cm})^{-1}$ x 10,000
13	1–2	360 nm sensitivity dN/dΩ, in $(\text{matm-cm})^{-1}$ x 10,000
	3–4	Effective Reflectivity, in percent x 100
14	1–2	Total Ozone, in matm-cm x 10
14	3–4	Error Flag (flag = flag + 10 for data taken during descending, N–S, orbit): 0 (10) good data 1 (11) good data, 84˚ < SZA < 88˚ 2 (12) pair residue too large 3 (13) triplet residue too large: use: 318 and 331 nm for A-triplet 331 and 340 nm for B-triplet 318 and 340 nm for C-triplet 4 (14) SOI flag set (SO_2 is present) 5 (15) fatal: set when the absolute value of any residue is larger than 12.5; ozone and SOI set to fill values
15	1	312 nm dN/dR (reflectivity sensitivity), in percent^{-1} x –50
	2	317 nm dN/dR, in percent^{-1} x –50
	3	331 nm dN/dR, in percent^{-1} x –50
	4	340 nm dN/dR, in percent^{-1} x –50
16	1	360 nm dN/dR, in percent^{-1} x –50
	2	380 nm dN/dR, in percent^{-1} x –50
	3	Cloud pressure measured by THIR, where available, in atm x 100
	4	Terrain pressure, in atm x 100
17	1	312 nm residue x 10 + 127

Table 7.8. Detailed Descriptions (Continued)

Word	Bytes	Description
	2	317 nm residue x 10 + 127
	3	331 nm residue x 10 + 127
	4	340 nm residue x 10 + 127
18	1	360 nm residue x 10 + 127
	2	Amount of ozone added below cloud layer, in matm-cm
	3	SOI, in matm-cm + 50
	4	Pressure derived from ISCCP cloud climatology, in atm x 100
19	1	Algorithm flag (flag = flag + 10 for snow assumed present): 1 (11) A-triplet used 2 (12) B-triplet used 3 (13) B-triplet used with profile selection 4 (14) C-triplet used with profile selection
	2	Effective cloud fraction x 100
	3	Profile mixing fraction x 10: $1 < f_p < 2$ profile between low and mid latitudes $2 < f_p < 3$ profile between low and mid latitudes
	4	Surface category code: 0 water 1 land 2 low inland (below sea level) 3 land and water 4 land and low-inland 5 water, land and low-inland
20–523		Same as 6–19 for samples 2–35
523–525		Spares

Table 7.9. Format of Orbital Summary Record

Word	Description
1	Orbit number
2	GMT (seconds) of first scan of orbit
3	Negative logical sequence number (2 most significant bytes)*
4	Day of year of first scan of orbit
5	Year of first scan of orbit (4 digits)
6	Latitude (90˚ S–90˚ N) for first scan, nadir view (degrees x 100)
7	Longitude (180˚ W–180˚ E) for first scan, nadir view (degrees x 100)
8	GMT (seconds) of last scan of orbit
9	Day of year of last scan of orbit
10	Year of last scan of orbit (4 digits)
11	Latitude (90˚ S–90˚ N) for last scan, nadir view (degrees x 100)
12	Longitude (180˚ W–180˚ E) for last scan, nadir view (degrees x 100)
13	Local time (seconds) at equator crossing (or –77 if unavailable)
14	Day of year (local time) at equator crossing
15	Year (local time) at equator crossing
16	GMT (seconds) at equator crossing (or –77 if unavailable)
17	Day of year (GMT) at equator crossing
18	Year (GMT) at equator crossing
19	Longitude at equator crossing (or –77777 if unavailable), nadir view (degrees x 100)
20	Altitude (km) at last scan
21	Number of input/output errors for this orbit

Table 7.9. Format of Orbital Summary Record (Continued)

Word	Description
22	Number of scans read for orbit
23	Number of scans written for orbit
24	Number of samples out of range (total)
	Number of samples out of range for:
25	Zenith angle > 88 degrees
26	Latitude out of range (> 90 degrees)
27	Counts negative
28	Number of bad samples written: algorithm flag not 0, 1, 10, or 11 (total)
29–34	Counts of error flags for Algorithm Flag = 1 (see data record for description of error flags):
29	number of samples that had error flag = 0 or 10
30	number of samples that had error flag = 1 or 11
31	number of samples that had error flag = 2 or 12
32	number of samples that had error flag = 3 or 13
33	number of samples that had error flag = 4 or 14
34	number of samples that had error flag = 5 or 15
35–40	Same as 29–34 for Algorithm Flag = 2
41–46	Same as 29–34 for Algorithm Flag = 3
47–52	Same as 29–34 for Algorithm Flag = 4
53	Minimum ozone for orbit.
54	Maximum ozone for orbit.
55–60	The six instrument wavelengths.
61–66	Solar irradiance F-values at 1 AU (watts/cm^3) for current day at the six instrument wavelengths, shortest first.
67–90	Calibration constants: The counts to radiance conversion factors, in units of watts/cm^3/steradian/count, given for each of the four gain ranges for each of the six wavelengths in order: words 63–66, 312 nm; ...; words 83–86, 380 nm.
91–127	Nominal spacecraft zenith angle (0–80 degrees) at each scan position.

* Notes: The logical sequence number is a 16-bit integer that occupies the left half (two most significant bytes) of word 3. Words 53–127 are stored in IEEE-754 32-bit floating-point format (REAL*4); all others are 4-byte (32-bit) integer format with the most significant byte first.

Table 7.10. Format of Trailer Record

Word	Description
1	Orbit number of last scan
2	GMT (seconds) of first scan of last orbit of day
3	Logical sequence number (= –1) (2 most significant bytes)*
4	Day of year of first scan of last orbit of day
5	Year of first scan of last orbit of day
6	Latitude (90˚ S–90˚ N) for first scan, nadir view (degrees x 100)
7	Longitude (180˚ W–180˚ E) for first scan, nadir view (degrees x 100)
8	GMT (seconds) of last scan of last orbit of day
9	Day of year of last scan of last orbit of day
10	Year of last scan of last orbit of day
11	Latitude (90˚ S–90˚ N) for last scan, nadir view (degrees x 100)
12	Longitude (180˚ W–180˚ E) for last scan, nadir view (degrees x 100)
13	Total number of input/output errors
14	Total number of scans read
15	Total number of scans written

Table 7.10. Format of Trailer Record (Continued)

Word	Description
16	Total number of good samples written
17	Total number of samples out of range
	Total number of samples out of range for:
18	Zenith angle > 85.7 degrees
19	Latitude out of range (absolute value > 90 degrees)—normally zero
20	Counts out of range (negative)
21	Number of samples written that were bad: algorithm flag not 0, 1, 10, or 11 (total)
22–27	Totals of error flag counts for algorithm flag = 1:
22	Total number of samples that had error flag = 0 or 10
23	Total number of samples that had error flag = 1 or 11
24	Total number of samples that had error flag = 2 or 12
25	Total number of samples that had error flag = 3 or 13
26	Total number of samples that had error flag = 4 or 14
27	Total number of samples that had error flag = 5 or 15
28–33	Same as 22–27 for Algorithm Flag = 2
34–39	Same as 22–27 for Algorithm Flag = 3
40–45	Same as 22–27 for Algorithm Flag = 4
46–525	Spare

* The trailer record identifier (= –1) is a 16-bit integer that occupies the left half (two most significant bytes) of word 3. All other values are stored as 4-byte integers, MSB first.

7.2.2 CDTOMS (Level–3 Data Product)

The CDTOMS Level–3 product contains global total ozone on a fixed 1-degree latitude by 1.25-degree longitude grid. It is available at URL ftp://jwocky.gsfc.nasa.gov/pub/meteor3/ or in the form of CD–ROMs. Except for some changes in the header line, the Version 7 Level–3 product is identical to the Nimbus–7/TOMS Version 6 CD–ROM product and the CDTOMS ozone product that was available by ftp.

One global grid is stored in each CDTOMS file. The first three lines in a CDTOMS daily grid file contain header information:

a) the date of observations (line 1; characters 2–22),
b) the processing version (line 1; characters 24–37),
c) the satellite/instrument name (line 1; characters 39–51),
d) the product name (line 1; 53–57),
e) local time of the ascending node equator crossing (line 1; characters 62–79), and
f) a description of the grid (lines 2 and 3).

Table 7.11 provides a detailed description of the first line of a daily grid file. The remaining lines contain the gridded ozone values, stored as 3-digit integers in units of matm-cm. Each of the 180 latitude zones requires 12 lines. They are ordered from south to north with the first zone centered at –89.5 degrees. Within each latitude zone, values are given for each of 288 longitude zones from 180˚ W through 0˚ (Greenwich) to 180˚ E. The first longitude zone is centered at –179.375 degrees. As shown in Figure 7.1 annotation is present after all values are given for a latitude zone. Zeroes denote flagged data; that is data that could not be collected due to lack of sunlight or other problems.

Figure 7.1 shows an example of the header and the first two latitude zones in a CDTOMS daily file from the Nimbus–7 TOMS.

Table 7.11. Format of Header Line of CDTOMS Daily Grid

Character	Contents
1	ASCII blank (HEX 20)
2–5	“Day:” (quotes indicate fixed content)
6	ASCII blank
7–9	day of year
10	ASCII blank
11–13	month (“Jan,” “Feb,” “Mar” ...)
14	ASCII blank
15–16	day of month
17	“,”
18	ASCII blank
19–22	year
23	ASCII blank 70
24–37	“Production V07”
38	ASCII blank
39–51	“METEOR–3/TOMS”
52	ASCII blank
53–57	“OZONE”
58–61	ASCII blanks
62–70	“Asc LECT:”
71	ASCII blank
72–73	hour (local) of ascending node equator crossing
74	ASCII “:”
75–76	minute (local) of ascending node equator crossing
77	ASCII blank
78–79	“AM” or “PM” indicating morning or afternoon/evening ascending node equator crossing
80	ASCII blank
81<	lf > (line feed character; i.e., HEX 0A)

```
Day: 336 Dec  1, 1992 Production V70 METEOR-3/TOMS OZONE    Asc LECT:  5:37 AM
Longitudes:  288 bins centered on 179.375 W to 179.375 E  (1.25 degree steps)
Latitudes  :  180 bins centered on  89.5   S to  89.5   N  (1.00 degreesteps)
211211211211207207207207205205205205205205205205205205205205205205205205205205205200200200
200199199199199197197197197195195195195194194194194194194194194194194194194194194194194194
194194194194194194187187187187189189189189192192192192192192192192192192192192192192192188
188188188188188188188188188188188188188188188188189189189189189189189189189189189189195195195195
195195195195195195195195195195195195195197197197197200200200200198198198198199199199199201201201
201201201201201201201201201202202202202202202202202192192192192192192192192192192192192192192
192192192192192192192192192192192208208208208208208208208208208208208208208208208208208208197
197197197197197197197197200200200200200200200200202202202202203203203203201201201201201201201201
201201201201201201201201201201201201201201201201197197197197199199199199198198198198196196196
196196196196196192192192192   lat =  -89.5
217217217217217217217217209209209209203203203203202202202202202202202202202202202202199199199
199198198198198191191191191191191191191191191191191191191191191191191191191191189189189189189189
189189189189189189186186186186186186186186187187187187187187187187187187187187187187187187
187187187188188188188190190190190190190190190190190190190190190190190190190190191191191191
192192192192192192192192192192192192192193193193193193193193200200200200200200200200200200
200200200200200201201201202202202202211211211211211211211211211211211211211211211211211
211211213213213213217217217217217217217217220220220220216216216216219219219219219219219219211
211211211211211211211209209209209221221221221220220220220218218218218218218218218217217217217
216216216216214214214214208208208208206206206206206206206206206206206206203203203203198198198
198196196196196196196196   lat =  -88.5
```

Figure 7.1. Sample CDTOMS Daily Grid File Excerpt

REFERENCES

Ahmad, Z. and P. K. Bhartia, 1995, "Effect of Molecular Anisotropy on the Backscattered UV Radiance," submitted to *Applied Optics*.

Bhartia, P. K., J. R. Herman, R. D. McPeters, and O. Torres, 1993, "Effect of Mount Pinatubo Aerosols on Total Ozone Measurements From Backscatter Ultraviolet (BUV) Experiments," *J. Geophys. Res.*, *98*, 18547–18554.

Cebula, R. P., H. Park, and D. F. Heath, 1988, "Characterization of the Nimbus–7 SBUV Radiometer for the Long-Term Monitoring of Stratospheric Ozone," *J. Atm. Ocean. Tech.*, *5*, 215–227.

Chu, W. P., M. P. McCormick, J. Lenoble, C. Brogniez, and P. Pruvost, 1989, "SAGE II Inversion Algorithm," *J. Geophys. Res.*, *94*, 8339–8351.

Dave, J. V., 1964, "Meaning of Successive Iteration of the Auxiliary Equation of Radiative Transfer," *Astrophys. J.*, *140*, 1292–1303.

Dave, J. V., 1978, "Effect of Aerosols on the Estimation of Total Ozone in an Atmospheric Column From the Measurement of its Ultraviolet Radiance," *J. Atmos. Sci*., *35*, 899–911.

Environmental Science Services Administration, National Aeronautics and Space Administration, and United States Air Force, 1966, *U. S. Standard Atmosphere Supplements*, U.S. Government Printing Office, Washington, DC.

Fleig, Albert J., R. D. McPeters, P. K. Bhartia, Barry M. Schlesinger, Richard P. Cebula, K. F. Klenk, Steven L. Taylor, and D. F. Heath, 1990, "Nimbus–7 Solar Backscatter Ultraviolet (SBUV) Ozone Products User's Guide," *NASA Reference Publication, 1234*, National Aeronautics and Space Administration, Washington, DC.

Heath, D. F., A. J. Krueger, H. R. Roeder, and B. D. Henderson, 1975, "The Solar Backscatter Ultraviolet and Total Ozone Mapping Spectrometer (SBUV/TOMS) for Nimbus G," *Opt. Eng.*, *14*, 323–331.

Heath, D. F., A.J. Krueger, and H. Park, 1978, "The Solar Backscatter Ultraviolet (SBUV) and Total Ozone Mapping Spectrometer (TOMS) Experiment," in *The Nimbus–7 Users' Guide*, edited by C. R. Madrid, 175–211, NASA Goddard Space Flight Center, Greenbelt, MD.

Ilg, D., F. Baker, and M. Folk, 1993, "HDF Specification and Developer's Guide, Version 3.2," National Center for Supercomputing Applications, Champaign, IL.

Jaross, G., A. J. Krueger, 1993, "Ice Radiance Method for Backscatter UV Instrument Monitoring," in *Atmospheric Ozone*, edited by T. Henriksen, 94–101, D. Reidel, Norwell, Mass.

Jaross, G., A. J. Krueger, R. P. Cebula, C. Seftor, U. Hartman, R. Haring, and D. Burchfield, 1995, "Calibration and Postlaunch Performance of the Meteor–3/TOMS Instrument," *J. Geophys. Res.*, *100*, 2985-2995.

Joiner, J., P. K. Bhartia, R. P. Cebula, E. Hilsenrath, and R. D. McPeters, 1995, "Rotational Raman Scattering (Ring Effect) in Satellite Backscatter Ultraviolet Measurements," *Applied Optics*, *34*, 4513-4525.

Kalman, L., 1994,"HDF Reference Manual, Version 3.3," National Center for Supercomputing Applications, Champaign, IL.

Klenk, K. F., P. K. Bhartia, A. J. Fleig, V. G. Kaveeshwar, R. D. McPeters, and P. M. Smith, 1982, "Total Ozone Determination From the Backscattered Ultraviolet (BUV) Experiment," *J. Appl. Meteorol.*, *21*, 1672–1684.

Klenk, K. F., P. K. Bhartia, E. Hilsenrath, and A. J. Fleig, 1983, "Standard Ozone Profiles From Balloon and Satellite Data Sets," *J. Climate Appl. Meteorol.*, *22*, 2012–2022.

McPeters, R., D., A. J. Krueger, P. K. Bhartia, J. R. Herman, A. Oakes, Z. Ahmad, R. P. Cebula, B. M. Schlesinger, T. Swissler, S. L. Taylor, O. Torres, and C. G. Wellemeyer, 1993, "Nimbus–7 Total Ozone Mapping Spectrometer (TOMS Data Products User's Guide," *NASA Reference Publication, 1323*, National Aeronautics and Space Administration, Washington, DC.

McPeters, R. D., et al., 1996. "Nimbus–7 Total Ozone Mapping Spectrometer (TOMS) Data Product's User's Guide," *NASA Ref. Publ. Planned*, National Aeronautics and Space Administration, Washington, DC.

NASA, 1993, "Interim Status Report on Results from the U.S./Russian Meteor–3/Total Ozone Mapping Spectrometer," NASA Technical Memorandum, 104576, National Aeronautics and Space Administration, Washington, DC.

National Center for Supercomputing Applications, 1994, "Hierarchical Data Format," http://www.ncsa.uiuc.edu/SDG/software/HDF/HDFIntro.html, hypertext file.

Paur, R. J., and A. M. Bass, 1985, "The Ultraviolet Cross-Sections of Ozone: II. Results and Temperature Dependence," *Atmospheric Ozone*, edited by C.S. Zerefos and A. Ghazi, 611–616, D. Reidel, Dordrecht.

Rottman, G. J., C. A. Barth, R. J. Thomas, G. H. Mount, G. M. Lawrence, D. W. Rusch, R. W. Saunders, G. E. Thomas, and J. London, 1982, "Solar Spectral Irradiance, 120 to 190 nm, October 13, 1981–January 3, 1982," *Geophys. Res. Lett.*, *9*, 587-593.

REFERENCES (Continued)

Torres, O., Z. Ahmad, and J. R. Herman, 1992, "Optical Effects of Polar Stratospheric Clouds on the Retrieval of TOMS Total Ozone," *J. Geophys. Res., 97*, 13,015–13,024.

Torres, O., and P. K. Bhartia, 1995, "Effect of Stratospheric Aerosol on Ozone Profile From BUV Measurements," *Geophys. Res. Lett., 22*, 235–238.

Torres, O., J. R. Herman, P. K. Bhartia, and Z. Ahmad, 1995, "Properties of Mount Pinatubo Aerosols as Derived From Nimbus–7 Total Ozone Mapping Spectrometer Measurements," *J. Geophys. Res., 100*, 14,043–14,055.

Wellemeyer, C. G., S. L. Taylor, G. Jaross, M. T. DeLand, C. J. Seftor, G. Labow, T. J. Swissler, and R. P. Cebula, 1996, "Final Report on Nimbus–7 TOMS Version 7 Calibration," *NASA Contractor Report 4717*, National Aeronautics and Space Administration, Washington, DC.

Woods, T. N., *et al.*, 1996, "Validation of the UARS Solar Ultraviolet Irradiance: Comparison With the Atlas 1–2 Measurements," *J. Geophys. Res.*, in press.

RELATED LITERATURE

Bates, D. R., 1984, "Rayleigh Scattering by Air," *Planet. Sp. Sci., 32,* 785–790.

Bhartia, P. K., K. F. Klenk, D. Gordon, and A. J. Fleig, "Nimbus–7 total Ozone Algorithm," 1983, *Proceedings, 5th Conference on Atmospheric Radiation,* American Meteorological Society, Baltimore, MD.

Bhartia, P. K., K. F. Klenk, C. K. Wong, D. Gordon, and A. J. Fleig, 1984, "Intercomparison of the Nimbus–7 SBUV/TOMS Total Ozone Data Sets With Dobson and M83 Results," *J. Geophys. Res., 89,* 5239–5247.

Bhartia, P. K., D. Silberstein, B. Monosmith, and Albert J. Fleig, 1985, "Standard Profiles of Ozone From Ground to 60 km Obtained by Combining Satellite and Ground Based Measurements," *Atmospheric Ozone*, edited by C. S. Zerefos and A. Ghazi, 243–247, D. Reidel, Dordrecht.

Bluth, G. J. S., S. D. Doiron, C. C. Schnetzler, A. J. Krueger, and L. S. Walter, 1992, "Global Tracking of the SO_2 Clouds From the June 1991 Mount Pinatubo Eruptions," *Geophys. Res. Lett., 19*, 151–154.

Bluth, G. J. S., S. D. Doiron, C. C. Schnetzler, A. J. Krueger, and L. S. Walter, 1993, "New Constraints on Sulfur Dioxide Emissions From Global Volcanism," *Nature*, 366, 327–329.

Bowman, K. P., 1986, "Interannual Variability of Total Ozone During the Breakdown of the Antarctic Circumpolar Vortex," *Geophys. Res. Lett., 13*, 1193–1196.

Bowman, K. P. and A. J. Krueger, 1985, "A Global Climatology of Total Ozone From the Nimbus–7 Total Ozone Mapping Spectrometer," *J. Geophys. Res., 90*, 7967–7976.

Bowman, K. P., 1988, "Global Trends in Total Ozone," *Science, 239*, 48–50.

Chandra, S., 1986, "The Solar and Dynamically Induced Oscillations in the Stratosphere," *J. Geophys. Res., 91*, 2719–2734.

Chandra, S., 1993, "Changes in Stratospheric Ozone and Temperature Due to the Eruption of Mt. Pinatubo," *Geophys. Res. Lett.*, 20, 33–36.

Chandra, S., and R. S. Stolarski, 1991, "Recent Trends In Stratospheric Total Ozone: Implications of Dynamical and El Chichón Perturbation," *Geophys. Res. Lett., 18*, 2277–2280.

Dave, J. V., 1965, "Multiple Scattering in a Non-Homogeneous, Rayleigh Atmosphere," *J. Atmos. Sci.*, *22*, 273–279.

Dave, J. V., and Carlton L. Mateer, 1967, "A Preliminary Study on the Possibility of Estimating Total Atmospheric Ozone From Satellite Measurements," *J. Atmos. Sci*., *24*, 414–427.

Eck, T. F., P. K. Bhartia, P. H. Hwang and L. L. Stowe, 1987, "Reflectivity of Earth's surface and Clouds in Ultraviolet From Satellite Observations," *J. Geophys. Res.*, *92*, 4287–4296.

Fraser, R. S., and Z. Ahmad, 1978, "The Effect Of Surface Reflection and Clouds on the Estimation of Total Ozone From Satellite Measurements." Fourth NASA Weather and Climate Program Science Review, *NASA Conf. Publ. 2076*, 247–252, National Aeronautics and Space Administration, Washington, DC, [NTIS N7920633].

Fleig, A. J., P. K. Bhartia, and David S. Silberstein, 1986, "An Assessment of the Long-Term Drift in SBUV Total Ozone Data, Based on Comparison With the Dobson Network," *Geophys. Res. Lett., 13*, 1359–1362.

Fleig, A. J., R. D. McPeters, P. K. Bhartia, Barry M. Schlesinger, Richard P. Cebula, K. F. Klenk, Steven L. Taylor, and D. F. Heath, 1990, "Nimbus–7 Solar Backscatter Ultraviolet (SBUV) Ozone Products User's Guide," *NASA Reference Publication, 1234*, National Aeronautics and Space Administration, Washington, DC.

Fleig, A. J., D. S. Silberstein, R. P. Cebula, C. G. Wellemeyer, P. K. Bhartia, and J. J. DeLuisi, 1989, "An Assessment of the SBUV/TOMS Ozone Data Quality, Based on Comparison With External Data," *Ozone in the Atmosphere, Proceedings of the Quadrennial Ozone Symposium 1988 and Tropospheric Ozone Workshops*, edited by R. D. Bojkov and P. Fabian, 232–237, A. Deepak, Hampton, VA.

Gleason, J. F., P. K. Bhartia, J. R. Herman, R. McPeters, P. Newman, R. S. Stolarski, L. Flynn, G. Labow, D. Larko, C. Seftor, C. Wellemeyer, W. D. Komhyr, A. J. Miller, and W. Planet, 1993, "Record Low Global Ozone in 1992," *Science, 260*, 523–526.

Heath, D. F., 1988, "Non-Seasonal Changes in Total Column Ozone From Satellite Observations," 1970–1986, *Nature, 332*, 219–227.

Heath, D. F., 1990, "Changes in the Vertical Distribution of Stratospheric Ozone and the Associated Global Scale Changes in Total Ozone From Observations With the Nimbus–7 SBUV Instrument; 1978-1986," *Proceedings of the International Ozone Symposium 1988 and Tropospheric Ozone Workshops*, edited by R. Bojkov and P. Fabian, 810, A. Deepak, Hampton, VA.

Herman, J. R., R. D. Hudson, and G. Serafino, 1990, "Analysis of the Eight-Year Trend in Ozone Depletion From Empirical Models of Solar Backscattered Ultraviolet Instrument Degradation," *J. Geophys. Res., 95*, 7403–7416.

RELATED LITERATURE (Continued)

Herman, J. R., R. McPeters, R. Stolarski, D. Larko, and R. Hudson, 1991, "Global Average Ozone Change From November 1978 to May 1990," *J. Geophys. Res., 96*, 17,279–17,305.

Herman, J. R., R. McPeters, and D. Larko, 1993, "Ozone Depletion at Northern and Southern Latitudes Derived From January 1979 to December 1991 Total Ozone Mapping Spectrometer Data," *J. Geophys. Res., 98*, 12,783–12,793.

Herman, J. R., D. Larko, 1994, "Nimbus–7/TOMS-November 1, 1978 to May 6, 1993: Low Ozone Amounts During 1992–1993 From Nimbus–7 and Meteor–3 Total Ozone Mapping Spectrometer," *J. Geophys. Res., 99*, 3483–3496.

Hudson, R. D., J. R. Herman, and G. Serafino, 1989, "On the Determination of Long-Term Trends From SBUV Ozone Data," *Ozone in the Atmosphere, Proceedings of the Quadrennial Ozone Symposium 1988 and Tropospheric Ozone Workshops*, edited by R. Bojkov and P. Fabian, 189–192. A. Deepak, Hampton, VA.

Klenk, K. F., 1980, "Absorption Coefficients of Ozone for the Backscatter UV Experiment," *Applied Optics, 19*, 236–242.

Komhyr, W. D., R. D. Grass, and R. K. Leonard, 1989, "Total Ozone, Ozone Vertical Distributions, and Stratospheric Temperatures at South Pole, Antarctica, in 1986 and 1987," *J. Geophys. Res., 94*, 11,429–11,436.

Krueger, A. J., 1983, Sighting of El Chichon Sulfur Dioxide Clouds With the Nimbus–7 Total Ozone Mapping Spectrometer. *Science, 220*, 1377–1378.

Krueger, A.J., L.S. Walter, P.K. Bhartia, C.C. Schnetzler, N.A. Krotkov, I. Sprod, and G.J.S. Bluth, 1995, Volcanic Sulfur Dioxide Measurements from the Total Ozone Mapping Spectrometer Instruments, *J. Geophys. Res.*, 100, 14057–14076.

Krueger, A. J., M. R. Schoeberl, and R. S. Stolarski, 1987, "TOMS Observations of Total Ozone in the 1986 Antarctic Spring," *Geophys. Res. Lett., 14*, 527–530.

Larko, D. E., L. W. Uccellini, and A. J. Krueger, 1986, "Atlas of TOMS Ozone Data Collected During the Genesis of Atlantic Lows Experiment (GALE)" *NASA-TM-87809,* 99 pp.

Lienesch, J. H. and P. K. K. Pandey, 1985, "The Use of TOMS Data in Evaluating And Improving The Total Ozone from TOVS Measurements," *Rep. NOAA-TR-NESDIS-23, Issue 22*, 3814–3828.

Logan, J. A., 1985, "Tropospheric Ozone: Seasonal Behavior, Trends, and Anthropogenic Influence," *J. Geophys. Res., 90*, 10,463–10,482.

Pommereau, J. P., F. Goutail, H. LeTexier, and T. S. Jorgensen, 1989, "Stratospheric Ozone and Nitrogen Dioxide Monitoring at Southern and Northern Polar Latitudes," *Our Changing Atmosphere, Proceedings of the 28th Liege International Astrophysical Colloquium*, edited by P. Crutzen. J.-C. Gerard, and R. Zander, University de Liege, Liege, Belgium.

Schoeberl, M. R., A. J. Krueger, and P. A. Newman, 1986, "The Morphology of Antarctic Total Ozone as Seen by TOMS—Total Ozone Mapping Spectrometer," *Geophys. Res. Lett., 13*, 1217–1220.

Schoeberl, M. R., P. K. Bhartia, E. Hilsenrath, and O. Torres, 1993, "Tropical Ozone Loss Following the Eruption of Mt. Pinatubo," *Geophys. Res. Lett., 20*, 29–32.

Solomon, S., 1990, "Antarctic Ozone: Progress Towards a Quantitative Understanding," *Nature, 347*, 347–354.

Stolarski, R. S., A. J. Krueger, M. R. Schoeberl, R. D. McPeters, P. A. Newman, and J. C. Alpert, 1986, "Nimbus–7 Satellite Measurements of the Springtime Antarctic Ozone Decrease," *Nature, 322*, 808–811.

Stolarski, R. S., 1992, "Observations of Global Stratospheric Ozone Change," *Ber. Bunsen Ges. Phys. Chem., 96*, 258–263.

Stolarski, R. S., P. Bloomfield, R. D. McPeters, and J. R. Herman, 1991, "Total Ozone Trends Deduced From Nimbus–7 TOMS Data," *Geophys. Res. Lett., 18*, 1015–1018.

Stolarski, R. S., L. Bishop, R. Bojkov, M. L. Chanin, V. Fioletev, V. Kircchoff, J. Zawodny, and C. Zerefos, 1992, "Ozone and Temperature Trends," in Scientific Assessment of Ozone Depletion; 1991, *WMO Rep. 25*, 2.1–2.30, World Meteorol. Organ., Geneva.

Stolarski, R. S., R. Bojkov, L. Bishop, C. Zerefos, J. Staehelin, and J. Zawodny, 1992, "Measured Trends in Stratospheric Ozone," *Science, 256*, 342–349.

Vigroux, Ernest, 1953, "Contribution a l'Etude Experimental de l'Aabsorption de l'Ozone," *Ann. Phys., Ser. 12, 8*, 709–762.

Vigroux, E., 1967, "Determination des Coefficients Moyen d'Absorption de l'Ozone en vue des Observations Concernant L'ozone Atmospherique a l'Aide Du Spectrometre Dobson," *Ann. Phys., Ser. 14, 2*, 209–215.

Watson, R. T., and Ozone Trends Panel, 1990, "Report of the International Ozone Trends Panel 1988," *Rep. 18*. Global Ozone Res. and Monit. Proj., World Meteorol. Organ., Geneva.

RELATED LITERATURE (Continued)

Wellemeyer, C. G., A. J. Fleig, and P. K. Bhartia, 1989, "Internal Comparisons of SBUV and TOMS Total Ozone Measurements," *Ozone in the Atmosphere, Proceedings of the International Ozone Symposium and Tropospheric Ozone Workshops*, edited by R. Bojkov and P. Fabian, 193–197, A. Deepak, Hampton, VA.

Wellemeyer, C. G., S. L. Taylor, R. R. Singh, and R. D. McPeters, 1992, "External Comparisons Of Reprocessed SBUV/TOMS Ozone Data," *Ozone in the Troposphere and Stratosphere, Proceedings of the Quadrennial Ozone Symposium*, edited by R. D. Hudson, 911–914, *NASA Conference Publication 3266,* Greenbelt, MD.

LIST OF ACRONYMS, INITIALS, AND ABBREVIATIONS

ASCII	American Standard Code for Information Interchange
A.U.	Astronomical Unit
BRDF	Bi-directional Reflectivity Distribution Function
CAO	Central Aerological Observatory
CD–ROM	Compact Disk–Read Only Memory
CDTOMS	Compact Disk TOMS Gridded Data
DAAC	Distributed Active Archive Center
D. U.	Dobson Units (= milliatmosphere-centimeters)
EOF	Empirical Orthogonal Functions
ESSA	Environmental Science Services Administration
EOSDIS	Earth Observing System Data Information System
FOV	Field-of-View
ftp	file transfer protocol
GMT	Greenwich Mean Time
GRIDTOMS	Gridded TOMS Tape
GSFC	Goddard Space Flight Center
HDF	Hierarchical Data Format
HDTOMS	High Density TOMS Tape
IAM	Interface Adapter Model
IFOV	Instantaneous Field-of-View
ISCCP	International Satellite Cloud Climatology Project
LECT	Local Equator Crossing Time
M3	Meteor–3 spacecraft
MSB	Most Significant Bit
N7	Nimbus–7 spacecraft
NASA	National Aeronautics and Space Administration
NCSA	National Center for Supercomputing Applications
netCDF	Network Common Data Form
NMC	National Meteorological Center
NOAA	National Oceanic and Atmospheric Administration
OPT	Ozone Processing Team
PMT	Photo-Multiplier Tube
PSC	Polar Stratospheric Cloud
SAGE	Stratospheric Aerosol and Gas Experiment

LIST OF ACRONYMS, INITIALS, AND ABBREVIATIONS (Continued)

SBUV	Solar Backscatter Ultraviolet
SDS	Scientific Data Set
SOI	Sulfur Dioxide Index
THIR	Temperature-Humidity Infrared Radiometer
TOMS	Total Ozone Mapping Spectrometer
URL	Uniform Resource Locator
UV	Ultraviolet

APPENDIX A STANDARD TEMPERATURE AND OZONE PROFILES

This appendix contains the standard temperature and ozone profiles used in the calculation of radiances discussed in Section 5. The profiles are described as a function of Umkehr layers. The boundaries of the layers, in pressure units, and the location of the midpoints of the layers are given in Table A.1. Table A.2 gives the temperature at the midpoint of each layer, and Table A.3 gives the column ozone, in units of matm-cm, for each layer. The three-digit and one-letter code identifies the total ozone and latitude of the profile. Profiles are provided for three latitude zones: 15 degrees, denoted L for low, 45 degrees, denoted M for mid, and 75 degrees, denoted H for high. The three-digit number is the total ozone, in units of matm-cm.

Table A.1. Umkehr Layers

Umkehr Layer Number	Layer Pressure (mb)	Pressure at Altitude of Midpoint	Layer Midpoint (km)
12	0.000–0.247	–	–
11	0.247–0.495	.350	56.5
10	0.495–0.990	.700	51.0
9	0.990–1.980	1.40	45.5
8	1.980–3.960	2.80	40.2
7	3.960–7.920	5.60	35.2
6	7.920–15.80	11.2	30.4
5	15.80–31.70	22.4	25.8
4	31.70–63.30	44.8	21.3
3	63.30–127.0	89.6	17.0
2	127.0–253.0	179.0	12.5
1	253.0–506.0	358.0	7.9
0	506.0–1013	716.0	2.8

Table A.2. TOMS Version 7 Standard Temperature Profiles

Profile	Umkehr Layer Number										
	0	1	2	3	4	5	6	7	8	9	> 9
225L	283.0	251.0	215.6	200.7	210.7	221.6	231.1	245.3	258.7	267.4	265.4
275L	283.0	251.0	215.9	203.5	211.9	222.5	231.1	245.3	258.7	267.4	265.4
325L	283.0	251.0	216.5	207.0	213.6	223.0	231.1	245.3	258.7	267.4	265.4
375L	283.0	251.0	216.0	210.0	216.0	224.0	231.1	245.3	258.7	267.4	265.4
425L	283.0	251.0	216.0	213.0	217.0	224.5	231.1	245.3	258.7	267.4	265.4
475L	283.0	251.0	216.0	216.0	219.0	225.0	231.1	245.3	258.7	267.4	265.4
125M	237.0	218.0	196.0	191.0	193.0	210.0	227.6	239.4	253.6	263.9	262.6
175M	260.0	228.0	201.7	198.0	202.1	214.3	227.6	239.4	253.6	263.9	262.6
225M	273.0	239.0	213.3	207.5	211.7	219.1	227.6	239.4	253.6	263.9	262.6
275M	273.0	239.0	217.1	212.2	214.9	220.4	227.6	239.4	253.6	263.9	262.6
325M	273.0	239.0	219.1	216.6	217.0	220.8	227.6	239.4	253.6	263.9	262.6
375M	273.0	239.0	220.2	219.0	219.0	221.9	227.6	239.4	253.6	263.9	262.6
425M	273.0	239.0	220.9	220.7	221.0	223.7	227.6	239.4	253.6	263.9	262.6
475M	273.0	239.0	221.5	222.5	222.7	224.4	227.6	239.4	253.6	263.9	262.6
525M	273.0	239.0	222.3	224.8	225.5	225.8	227.6	239.4	253.6	263.9	262.6
575M	273.0	239.0	225.0	227.0	227.0	227.0	227.6	239.4	253.5	263.9	262.6
125H	237.0	218.0	196.0	191.0	193.0	210.0	223.3	237.1	251.6	262.4	265.6
175H	260.0	228.0	201.7	198.0	202.1	214.3	223.3	237.1	251.6	262.4	265.6
225H	260.0	228.0	209.7	208.5	212.5	222.0	228.0	237.1	251.6	262.4	265.6

Table A.2. TOMS Version 7 Standard Temperature Profiles (Continued)

Profile	Umkehr Layer Number										
	0	1	2	3	4	5	6	7	8	9	> 9
275H	260.0	228.0	222.6	223.4	223.8	226.5	231.6	237.1	251.6	262.4	265.6
325H	260.0	228.0	222.6	223.4	223.8	226.5	231.6	237.1	251.5	262.4	265.6
375H	260.0	228.0	222.6	223.4	223.8	226.5	231.6	237.1	251.5	262.4	265.6
425H	260.0	228.0	222.6	223.4	223.8	226.5	231.6	237.1	251.5	262.4	265.6
475H	260.0	228.0	222.6	223.4	223.8	226.5	231.6	237.1	251.5	262.4	265.6
525H	260.0	228.0	222.6	223.4	223.8	226.5	231.6	237.1	251.5	262.4	265.6
575H	260.0	228.0	222.6	223.4	223.8	226.5	231.6	237.1	251.5	262.4	265.6

Table A.3. TOMS Version 7 Standard Ozone Profiles

	Umkehr Layer Number										
Profile	0	1	2	3	4	5	6	7	8	9	> 9
225L	15.0	9.0	5.0	7.0	25.0	62.2	57.0	29.4	10.9	3.2	1.3
275L	15.0	9.0	6.0	12.0	52.0	79.2	57.0	29.4	10.9	3.2	1.3
325L	15.0	9.0	10.0	31.0	71.0	87.2	57.0	29.4	10.9	3.2	1.3
375L	15.0	9.0	21.0	53.0	88.0	87.2	57.0	29.4	10.9	3.2	1.3
425L	15.0	9.0	37.0	81.0	94.0	87.2	57.0	29.4	10.9	3.2	1.3
475L	15.0	9.0	54.0	108.0	100.0	87.2	57.0	29.4	10.9	3.2	1.3
125M	6.0	5.0	4.0	6.0	8.0	31.8	28.0	20.0	11.1	3.7	1.4
175M	8.0	7.0	8.0	12.0	26.0	41.9	33.6	22.3	11.1	3.7	1.4
225M	10.0	9.0	12.0	18.0	44.0	52.1	39.2	24.5	11.1	3.7	1.4
275M	16.0	12.0	15.0	29.0	58.0	63.7	40.6	24.5	11.1	3.7	1.4
325M	16.0	14.0	26.0	45.0	74.7	66.9	41.7	24.5	11.1	3.7	1.4
375M	16.0	16.0	39.0	64.0	85.7	71.1	42.5	24.5	11.1	3.7	1.4
425M	16.0	18.0	54.0	84.0	97.7	71.7	42.9	24.5	11.1	3.7	1.4
475M	16.0	22.0	72.0	107.7	101.0	72.6	43.0	24.5	11.1	3.7	1.4
525M	16.0	26.0	91.0	127.7	108.0	72.6	43.0	24.5	11.1	3.7	1.4
575M	16.0	30.0	110.0	147.7	115.0	72.6	43.0	24.5	11.1	3.7	1.4
125H	9.5	7.0	18.3	7.6	8.2	28.6	22.0	12.4	7.7	2.5	1.2
175H	9.5	8.0	22.8	22.0	26.9	32.3	26.8	15.0	8.0	2.5	1.2
225H	10.0	9.0	27.6	45.7	41.0	35.0	28.8	15.4	8.3	2.9	1.3
275H	14.0	12.0	34.0	66.9	54.2	36.0	28.8	15.4	8.9	3.4	1.4
325H	14.0	15.0	46.8	82.6	65.2	41.7	28.8	17.2	8.9	3.4	1.4
375H	14.0	20.0	61.2	93.8	75.2	45.9	32.5	18.7	8.9	3.4	1.4
425H	14.0	25.0	76.2	104.9	84.2	51.4	35.6	20.0	8.9	3.4	1.4
475H	14.0	32.0	91.0	117.1	93.0	55.8	37.5	20.9	8.9	3.4	1.4
525H	14.0	41.0	107.1	128.1	101.0	60.2	38.2	21.7	8.9	3.4	1.4
575H	14.0	49.0	123.2	142.2	111.0	60.6	38.8	22.5	8.9	3.4	1.4

APPENDIX B. SOFTWARE TO READ HDF OZONE DATA

This appendix describes software that can be used to read the TOMS HDF Level–2 and Level–3 data files. The software is written in C and requires the HDF version 3.3 or 4 (or higher) libraries to compile. The read software is available at the GSFC DAAC (see Appendix C). The HDF libraries can be downloaded via anonymous ftp at ftp.ncsa.uiuc.edu in directory /HDF. Copies of the most recent HDF version libraries can be downloaded from the DAAC anonymous ftp server at daac.gsfc.nasa.gov in directory /pub/hdf.

The Program read_tomsl2.c can be used to read the TOMS Level–2 HDF files. Issuing the command read_tomsl2 will display a list of the HDF files in the current directory. Next, the program will display the following information:

- Text: “File description stored in the file” (optional)
- A prompt to save the output to an ASCII file
- File label and metadata

The next keystroke will display netCDF-style global attributes.

The next keystroke will display a numbered list of all the SDSs providing the name and dimensions of the SDS corresponding to each number. The user can select any SDS to view, or can exit the program by entering q. For the selected SDS, the program will display a description of the axis or axes, the physical units, and offsets and scale factors used to convert the values in the HDF data set to physical values. The user can then press q or any other key to go back to the SDS list and continue browsing the data. After selecting the desired SDS, the user can then select a latitude band for which the data will be displayed. The output will include year, day number, time, latitude, longitude, solar zenith angle, scan number, nadir angle, and the SDS data. The output will be displayed in physical values.

The program read_tomsl3.c can be used to read the TOMS Level–3 HDF files. Issuing the command read_tomsl3 will display a list of the HDF files in the current directory. Next, the program will display the following information:

- File label
- Text: “File description stored in the file” (optional)
- Metadata

The next keystroke will display a numbered list of all the SDSs providing the name and dimensions of the SDS corresponding to each number: 1 is ozone, 4 is reflectivity. (Numbers 2 and 3 are coordinate data sets and will not be displayed by this software.) The user can display either SDS by entering its number or can exit the program by entering q. The user will be prompted to output the file to the screen, an ASCII file, or to a binary file. The output will be displayed in physical values. For screen and ASCII dumps, latitude and longitude values will be included with the data values.

APPENDIX C. DATA AVAILABILITY

The derivative data products defined in this User's Guide are archived at and available from the NASA Goddard Space Flight Center Distributed Active Archive Center (NASA/GSFC/DAAC). All data and services offered by the Goddard DAAC are free. For very high volume data orders, users may be asked to provide the magnetic tapes for the requested data.

The DAAC may be accessed on World Wide Web at http://daac.gsfc.nasa.gov/. Options for locating and accessing data are listed on the DAAC home page. Information about TOMS and other ozone data archived at the Goddard DAAC can be found at http://daac.gsfc.nasa.gov/CAMPAIGN_DOCS/ATM_CHEM/ac_main.html. In addition to data, the DAAC Web pages contain information about HDF, the format in which it provides the Level–2 and Level–3 TOMS products, available from ftp://daac.gsfc.nasa.gov/pub/hdf/. Get the README file.

The DAAC maintains a help desk, which provides assistance with its on-line ordering services. It can be reached as follows:

Electronic Mail:daacuso@daac.gsfc.nasa.gov
Telephone: +1-301-614-5224
FAX: +1-301-614-5268

The postal address of the DAAC is

Goddard Distributed Active Archive Center
Global Change Data Center

Code 902.2

NASA/Goddard Space Flight Center
Greenbelt, MD 20771

ABSTRACT

Two data products from the Total Ozone Mapping Spectrometer (TOMS) onboard Meteor–3 have been archived at the Distributed Active Archive Center, in the form of Hierarchical Data Format files. The instrument measures backscattered Earth radiance and incoming solar irradiance; their ratio is used in ozone retrievals. Changes in the reflectivity of the solar diffuser used for the irradiance measurement are monitored using a carousel of three diffusers, each exposed to the degrading effects of solar irradiation at different rates. The algorithm to retrieve total column ozone compares measured Earth radiances at sets of three wavelengths with radiances calculated for different total ozone values, solar zenith angles, and optical paths. The initial error in the absolute scale for TOMS total ozone is 3 percent, the one standard deviation random error is 3 percent, and drift is less than 0.5 percent over the course of the data record from August 22, 1991 through December 28, 1994. The Level–2 product contains the measured radiances, the derived total ozone amount, and reflectivity information for each scan position. The Level–3 product contains daily total ozone and reflectivity in a 1-degree latitude by 1.25 degrees longitude grid. The Level–3 product is also available on CD–ROM. Detailed descriptions of both HDF data files and the CD–ROM product are provided.

Total Ozone Mapping Spectrometer
Ozone
Reflectivity
Unclassified
Unclassified
Unclassified-Unlimited
Subject Category 46